Demand and Interference Aware Adaptive Resource Management for High Throughput GEO Satellite Systems

TEDROS SALIH ABDU (Graduate Student Member, IEEE), STEVEN KISSELEFF (Member, IEEE), EVA LAGUNAS (Senior Member, IEEE), SYMEON CHATZINOTAS (Senior Member, IEEE), AND BJÖRN OTTERSTEN (Fellow, IEEE)

Interdisciplinary Centre for Security, Reliability and Trust, University of Luxembourg, 1855 Luxembourg, Luxembourg

CORRESPONDING AUTHOR: T. S. ABDU (e-mail: tedros-salih.abdu@uni.lu)

ABSTRACT The scarce spectrum and power resources, the inter-beam interference, together with the high traffic demand, pose new major challenges for the next generation of Very High Throughput Satellite (VHTS) systems. Accordingly, future satellites are expected to employ advanced resource/interference management techniques to achieve high system spectrum efficiency and low power consumption while ensuring user demand satisfaction. This paper proposes a novel demand and interference aware adaptive resource management for geostationary (GEO) VHTS systems. For this, we formulate a multi-objective optimization problem to minimize the total transmit power consumption and system bandwidth usage while matching the offered capacity with the demand per beam. In this context, we consider resource management for a system with full-precoding, i.e., all beams are precoded; without precoding, i.e., no precoding is applied to any beam; and with partial precoding, i.e., only some beams are precoded. The nature of the problem is non-convex and we solve it by jointly using the Dinkelbach and Successive Convex Approximation (SCA) methods. The simulation results show that the proposed method outperforms the benchmark schemes. Specifically, we show that the proposed method requires low resource consumption, low computational time, and simultaneously achieves a high demand satisfaction.

INDEX TERMS Demand satisfaction, Dinkelbach method, high throughput GEO Satellite, precoding, radio resource management technique, successive convex approximation.

I. INTRODUCTION

THE NUMBER of connected devices and the high traffic demands needed by the end-users are on the rise in the satellite communication industry. It is challenging to accommodate this increasing demand using traditional and conventional resource assignment methods [2]. Furthermore, the limited satellite resources and the signal interference among the users restricts the data rates that the system can deliver. Therefore, signal processing techniques need to be employed in satellite payloads to mitigate the interference and to manage the satellite resources efficiently. Thanks to reconfigurable digital payload technologies, it is possible to

flexibly control the satellite resources [3]. Hence, to meet the increasing demand the following must be implemented on future broadband satellites:

1) Advanced radio resource management: the satellite resources should be distributed according to the heterogeneous user demand in order to achieve high demand satisfaction [2].

2) Advanced interference management techniques: aggressive frequency sharing strategies offer wide bandwidths without the need to acquire new spectrum licenses. However, this method creates additional interference among the adjacent beams, which

deteriorates the desired signal quality per user. Therefore, along with radio resource management, advanced interference management is required [4].

3) Computationally efficient algorithms: Adaptive Resource Control (ARC) is performed at the ground segment and should be fast enough to cope with the time-variant link conditions and major demand variations [5].

In this paper, we propose demand and interference aware adaptive resource management techniques for VHTS geostationary (GEO) satellite systems where three different key performance indicators are combined in a multi-objective mathematical formulation. These are: (1) user demand satisfaction; (2) transmit power; and (3) total operational bandwidth. Thus, we can optimize satellite resource utilization while matching heterogeneous traffic demands. Consequently, less power and bandwidth is needed in low-demand scenarios, while more power and bandwidth is needed in high-demand scenarios.

A. RELATED WORK

Several methods regarding power and/or bandwidth optimization have been studied in the literature for non-interference-limited scenarios. Analytical power optimization to satisfy the per beam demand has been considered in [6]–[10]. Furthermore, power allocation based on meta-heuristic and machine learning approaches has been proposed in [11]–[13] and [14]–[18], respectively. However, in these methods, demand-based bandwidth allocation is not considered. In contrast, demand-aware bandwidth allocation has been considered in [19]–[24]. However, in these methods, a fixed power is assumed regardless of the user demand. The shortcomings of the above techniques have been addressed by optimizing jointly the system power and bandwidth using a heuristic method in [25]–[27], and machine learning techniques in [28]–[31]. However, these techniques suffer from local optimally, which leads to lower demand satisfaction. Hence, there is no guarantee to attain a close-to-optimum solution. Generally, despite the availability of satellite resources, machine learning and meta-heuristic techniques cannot guarantee high-demand matching when there are insufficient training data and insufficient exploration-exploitation. In [32]–[34], joint power and bandwidth optimization have been proposed based on iterative convex optimization to utilize the satellite resource efficiently. However, these methods have high computational time due to the higher dimensionality of the optimization variables.

Recently, the adoption of aggressive frequency reuse is gaining momentum due to the new trends in satellite broadband traffic [35]. Accordingly, the interference becomes the limiting factor and needs to be mitigated by employing advanced signal processing techniques. In this context, precoding has become a popular interference mitigation technique for such interference-limited scenarios. In addition, the demand satisfaction can be further maximized using resource allocation.

The use of linear precoding techniques for satellite systems has been suggested in [36]–[38], and it has been recently tested over a real satellite link in [39]. The detail structure on finding the optimal linear precoder has been studied in [40]. The performance of linear precoding for the hotspot scenario has been studied in [41], where precoding is applied to direct the available satellite resource to a beam with very high traffic demand (hot-spot beam). However, the total transmit power is not optimized based on the per-user demand requirement.

The max-min fairness-based power optimization for the multicast-multigroup scenario has been considered in [42]. Later, the author proposed frame-based precoding under power antenna constraint to maximize the system capacity [43]. Similarly, to maximize the system capacity, multicast precoding with feeder link interference has been proposed [44]. However, the focus of the aforementioned methods is on system capacity maximization only, which may not be optimal with respect to the demand satisfaction. In [45], [46], a precoding design for an energy-efficient system has been considered under total power and quality of service constraints. However, the transmit power per beam constraint is not accounted for in the optimization. Furthermore, the power allocation is determined independently from demand. Hence, the algorithm does not adapt to the demand variations.

In the literature, very few works have addressed the Minimum Mean Square Error (MMSE) linear precoder combined with demand-aware resource allocation [47], [48]. However, in these methods, the power allocation flexibility is limited because the MMSE precoder considered the system's total power. Moreover, [47] and [48] focus on scheduling and beam hopping, respectively. In this paper, we focus on the frequency flexible rather than a time-flexible payload, for two reasons: 1) frequency-flexible payloads are more developed than beam-hopping payloads and seem to dominate the market at the moment; 2) to reduce the synchronization issues associated with non-continuous transmissions, which typical appear in beam-hopping systems.

Generally, the state-of-the-art precoding techniques assume full bandwidth utilization regardless of the user demand.[1] Herein, we focus on flexible bandwidth and power allocation to investigate the possible scenario where the satellite resources are optimized depending on demand without precoding. For this, we foresee a case where the traffic requested by a specific user is low; thus, the user may be able to tolerate some additional interference without precoding. Additionally, we consider a system with full-precoding, i.e., all beams are precoded and with partial precoding, i.e., only some beams are precoded on the

---

1. Typically full bandwidth implies 500 MHz in exclusive Ka band, or 2.5 GHz when both exclusive and non-exclusive Ka band is considered [49].

TABLE 1. Comparison of schemes.

		Payload Flexibility		Joint Resource Efficiency and User satisfaction			Optimization		
		Power	Bandwidth	Demand Matching	Total Power Minimization	Utilized BW Minimization	Without Precoding	With Full Precoding	With Partial Precoding
Machine Learning Optimization	[14]–[18]	✓					✓		
	[21]–[24]		✓				✓		
	[28]–[31]	✓	✓		✓		✓		
Heuristic Optimization	[26], [27]	✓	✓				✓		
	[11]–[13]	✓					✓		
Analytical Optimization	[6]–[10]	✓					✓		
	[19], [20], [25]		✓				✓		
	[33]	✓	✓				✓		
	[32], [34]	✓	✓		✓		✓		
	[42]–[48]	✓						✓	
	This work	✓	✓		✓		✓	✓	✓

top of resources optimization in case of high user demand and strong interference among the users.

Table 1 summarizes the difference between this work and the existing literature methods regarding (i) Payload flexibility (power or/and frequency); (ii) Joint resource efficiency, and user satisfaction optimization (demand matching, utilized BW minimization, and total power minimization); (iii) system precoding capability. From Table 1, we can observe that our work focuses on designing an algorithm that can control the resource of the satellite and interference signal among users according to the user demand and channel condition in order to provide high demand satisfaction with minimum resource utilization. Hence, unlike ([6]–[18], [21]–[24], [42]–[48]), this paper has power and bandwidth controlling flexibility and it differs from ([6]–[18], [21]–[24], [33], [42]–[48]), because this work jointly considers system efficiency and user satisfaction. Further, the proposed method includes precoding optimization flexibility, which differs from the previous works.

B. CONTRIBUTIONS

1) We formulate a multi-objective optimization problem for a system (i) with full-precoding for strong interference scenarios, (ii) with no precoding for low interference scenarios, (iii) with partial precoding that achieves the tradeoff between full-precoding and no precoding.

2) The novelty of the above optimization problems lies in the joint minimization of utilized bandwidth, total transmit power, and unmet system capacity under minimum SINR constraint, beam power constraint, and bandwidth per beam constraint. Hence, the system matches the demands while minimizing the total resource utilization. Furthermore, the problem is formulated to have a lower dimension of decision variables, thus reducing the computational complexity compared to the existing works.

3) The formulated problem is non-convex, such that it is difficult to obtain an optimal solution. Hence, to tackle the problem, first, we reformulate it in a more tractable form. Then, we apply Dinkelbach and SCA methods. For this, we propose an algorithm that allocates resources according to the demand and the channel condition. Consequently, the system has full flexibility to control its resources. Furthermore, the algorithm is designed to execute the Dinkelbatch method and SCA method simultaneously rather than alternatingly or as a concatenation of each other. Hence, the algorithm computational time decreases.

4) We show that the algorithm has polynomial time complexity and provide a detailed complexity analysis.

5) Finally, the proposed method demonstrates significant performance improvements using the simulation results in terms of resource utilization, demand satisfaction, computational time and convergence time.

The remainder of the paper is organized as follows. Section II introduces the system model. The proposed resource optimization is discussed in Section III. Section IV and Section V provides the simulation results and the conclusion, respectively. Finally, Section VI discusses future work.

Notation: Matrix and vector are represented by boldfaced upper case and lower case letters, respectively. The transpose of a vector and conjugate transpose of a vector represented by $[.]^T$ and $[.]^H$, respectively. Lastly, $|.|$ and $\|.\|_2$ denote the cardinality and the l_2-norm of a vector , respectively.

II. SYSTEM MODEL

We consider a downlink of a high throughput GEO satellite system operating in Ka-band with N spot beams. The generation of beams can be performed considering advanced on-board beamforming strategies or with conventional single-feed-per-beam architectures. The resulting spot beams overlap so that there are no holes in the coverage area of the considered GEO satellite system. Due to the side lobes of the multispot beam satellite footprint, the system becomes interference-limited. Conventional systems overcome the interference-limited scenario by employing the so-called four color frequency reuse (4CR), where the system bandwidth is divided into two carriers and operated with two different polarizations to generate, which results in four orthogonal communication channels.

With the motivation to increase the achievable data rate in order to face up the increasing traffic demands, in this work we consider a full frequency reuse (FFR) scheme where the same frequency is used by all beams of the system. Further, we define P_{total} and B_{total} as the total available transmit

power and system bandwidth, respectively. Depending on the intensity of the traffic demand, the system may not require the use of the whole B_{total}, but only a bandwidth chunk $B \leq B_{total}$. Furthermore, a single user per beam is served at a particular time instance, i.e., this user represents the beam aggregated traffic demand. Since both the desired signal and interference strongly depend on the users' location, in Section IV, we evaluate the proposed algorithms for different users' location.

Let the channel matrix $\mathbf{H} \in \mathbb{C}^{N \times N}$ is defined as $\mathbf{H} = [\mathbf{h}_1, \mathbf{h}_2, \ldots, \mathbf{h}_N]^H$, where $\mathbf{h}_i \in \mathbb{C}^{N \times 1}$ is the channel vector from the satellite to the ith user is defined as $\mathbf{h}_i = [h_i[1], h_i[2], \ldots, h_i[N]]^H$. Following previous works [43], [50], we assume a clear sky channel condition where the atmospheric attenuation is negligible. Hence, the satellite channel is mainly defined by the line-of-sight component of the signal and the antenna pattern. In this context, the channel coefficient $h_i[j]$ is given by

$$h_i[j] = \frac{\sqrt{G_R G_i[j]}}{4\pi \frac{d_i}{\lambda}} e^{-j\phi_i}, \quad (1)$$

where ϕ_i is the phase component introduced by the the satellite antenna, G_R is the user terminal antenna gain, $G_i[j]$ denotes the gain from the jth satellite beam towards the beam i user, λ is the carrier wavelength and d_i is the slant range between the satellite and the ith user.

We consider the system to handle K beams with precoding and $L = N - K$ beams without precoding. The K beams are categorized for precoding into disjoint groups and the set of groups is defined as $\mathcal{K} = \{\mathcal{K}_1, \mathcal{K}_2, \ldots, \mathcal{K}_m, \ldots, \mathcal{K}_M\}$, where $\mathcal{K}_m$ is the mth group of beams. Furthermore, a set that contain L non-precoded beams is denoted as $\mathcal{L}$. The channel matrix $\hat{\mathbf{H}}_m \in \mathbf{H}$ for $\mathcal{K}_m$ is defined as $\hat{\mathbf{H}}_m = [\hat{\mathbf{h}}_{k,m}[m]]_{k \in \mathcal{K}_m}^H$, where $\hat{\mathbf{h}}_{k,m}[m] \in \mathbb{C}^{|\mathcal{K}_m| \times 1}$ is the channel vector from the satellite to user in beam k belonging to the mth group and $|\mathcal{K}_m|$ is the cardinality of the mth group. Furthermore, the interference channel vector received by the k user of $m$the group from the $z \neq m$ group is denoted as $\hat{\mathbf{h}}_{k,m}[z] \in \mathbb{C}^{|\mathcal{K}_z| \times 1}$. For instance, from Fig. 1, the colored beams are categorized for precoding and we obtain the set of groups $\mathcal{K}$ as $\mathcal{K} = \{\mathcal{K}_1, \mathcal{K}_2\}$, where $\mathcal{K}_1 = \{2, 6\}$ and $\mathcal{K}_2 = \{1, 5\}$. The channel matrix for $\mathcal{K}_1$ is given by $\hat{\mathbf{H}}_1 = [\hat{\mathbf{h}}_{2,1}[1], \hat{\mathbf{h}}_{6,1}[1]]^H$, where $\hat{\mathbf{h}}_{2,1}[1] = [h_2[2], h_2[6]]^H$, and $\hat{\mathbf{h}}_{6,1}[1] = [h_6[2], h_6[6]]^H$. The interference channel vector received by user in beam 2 and 6 from $\mathcal{K}_2$ is $\hat{\mathbf{h}}_{2,1}[2] = [h_2[1], h_2[5]]^H$ and $\hat{\mathbf{h}}_{6,1}[2] = [h_6[1], h_6[5]]^H$, respectively. Similar to $\mathcal{K}_1$, the channel matrix for $\mathcal{K}_2$ is given by $\hat{\mathbf{H}}_2 = [\hat{\mathbf{h}}_{1,2}[2], \hat{\mathbf{h}}_{5,2}[2]]^H$, where $\hat{\mathbf{h}}_{1,2}[2] = [h_1[1], h_1[5]]^H$, and $\hat{\mathbf{h}}_{5,2}[2] = [h_5[1], h_5[5]]^H$. The interference channel vector received by user in beam 1 and 5 from $\mathcal{K}_1$ is $\hat{\mathbf{h}}_{1,2}[1] = [h_1[2], h_1[6]]^H$ and $\hat{\mathbf{h}}_{5,2}[1] = [h_5[2], h_5[6]]^H$, respectively.

The precoding matrix for the mth group is denoted as $\hat{\mathbf{W}}_m = [\hat{\mathbf{w}}_{k,m}[m]]_{k \in \mathcal{K}_m}^T$, where $\hat{\mathbf{w}}_{k,m}[m] \in \mathbb{C}^{|\mathcal{K}_m| \times 1}$ is the precoding weight vector for the user in beam k belonging
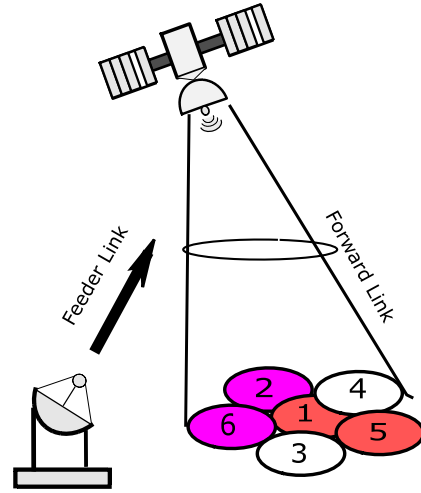

FIGURE 1. The system with six beams with $\mathcal{K}_1 = \{2, 6\}$, $\mathcal{K}_2 = \{1, 5\}$, and $\mathcal{L} = \{3, 4\}$.

to the mth group. For example, the precoding matrix for $\mathcal{K}_1$ group is $\hat{\mathbf{W}}_m = [\hat{\mathbf{w}}_{2,1}[1], \hat{\mathbf{w}}_{6,1}[1]]^T$, where $\hat{\mathbf{w}}_{2,1}[1] = [w_2[2], w_2[6]]^T$, and $\hat{\mathbf{w}}_{6,1}[1] = [w_6[2], w_6[6]]^T$.

Then, the received signal-to-interference-plus-noise ratio (SINR) for the lth non-precoded user and the kth precoded user in the mth group is given by

$$\gamma_l = \frac{g_{l,l}p_l}{\left(\sum_{j \in \mathcal{L}, j \neq l} g_{l,j}p_j + \sum_{K_z \in \mathcal{K}} \sum_{j \in \mathcal{K}_z} |\hat{\mathbf{h}}_{l,z}^H[z]\hat{\mathbf{w}}_{j,z}[z]|^2 + N_0 B \right)}, \quad (2)$$

$$\gamma_{k,m} = \frac{|\hat{\mathbf{h}}_{k,m}^H[m]\hat{\mathbf{w}}_{k,m}[m]|^2}{\left(\sum_{K_z \in \mathcal{K}} \sum_{j \in \mathcal{K}_z, j \neq k} |\hat{\mathbf{h}}_{k,m}^H[z]\hat{\mathbf{w}}_{j,m}[z]|^2 + \sum_{l \in \mathcal{L}} g_{k,l}p_l + N_0 B \right)}, \quad (3)$$

where p_l is the transmit power for the user in beam l, N_0 is the noise spectral density, $g_{l,j} = |h_l[j]|^2, \forall l, j \in \mathcal{L}$ is the interference channel power gain from non-precoded jth beam to the non-precoded user in beam l, and $\hat{\mathbf{h}}_{l,z}[z]$ is the received channel interference vector by the non-precoded user in beam l from the precoded user's of z group. For example, interference signal received by the non-precoded beams: $\mathcal{L} = \{3, 4\}$ from $\mathcal{K}_1$ is $\hat{\mathbf{h}}_{3,1}[1] = [h_3[2], h_3[6]]^H$, and $\hat{\mathbf{h}}_{4,1}[1] = [h_4[2], h_4[6]]^H$, respectively.

Hence, the offered capacity to user in beam i is

$$C_i = B \log_2(1 + \gamma_i), \quad (4)$$

where

$$\gamma_i = \begin{cases} \gamma_l & \text{if } i = l, l \in \mathcal{L} \\ \gamma_{k,m} & \text{if } i = k, k \in \mathcal{K}_m. \end{cases} \quad (5)$$

Finally, given the user in beam i demand D_i, the normalized unmet system capacity is given by

$$C_{\text{unmet}} = \sum_{i=1}^{N} \max(1 - C_i/D_i, 0). \quad (6)$$

From the system model, we can observe the following scenarios:

1) The system without precoding: This occurs when $|\mathcal{K}| = 0$, which indicates that no precoding is applied to any users. The computational complexity of the system without precoding is lower because no precoder design is required. However, the spectral efficiency that can be obtained without precoding is limited due to the interference signal among the users. The lower spectral efficiency results in higher C_{unmet}. Hence, the overall resource utilization may not be efficient for high demand and strong interference if no precoding is employed.

2) The system with full-precoding: This occurs with $|\mathcal{K}_m| = N$, which indicates that all users are fully precoded. The full-precoding method mitigates the interference signal among the users which results in higher spectral efficiency. Hence, we obtain lower C_{unmet}. However, full-precoding requires the design of a $N \times N$ precoder matrix that may increase the system complexity.

3) The system with partial precoding: This occurs when $|\mathcal{K}_m| < N, \forall_m$. Using partial precoding,[2] we can address the tradeoff between complexity and spectral efficiency of the system.

III. PROPOSED RESOURCE OPTIMIZATION

In this section we formulate the resource management optimization problem for high throughput geostationary (GEO) satellite systems where three different key performance indicators are combined in a multi-objective mathematical formulation. These are: (1) user demand satisfaction; (2) transmit power; and (3) total operational bandwidth. For this, we consider a joint minimization of the unmet system capacity C_{unmet}, the transmit power p_l, the transmit power $\|\hat{\mathbf{w}}_{k,z}[z]\|_2^2$ for the $\hat{\mathbf{w}}_{k,z}[z]$ and the bandwidth utilization B. Consequently, we can closely match the offered capacity and the requested demand to ensure high demand satisfaction while using minimum overall power and bandwidth consumption. Hence, the formulated problem is shown as follows

$$
\begin{aligned}
\underset{\substack{B, p_l, \forall_l, \\ \hat{\mathbf{w}}_{k,z}[z], \forall_k \in \mathcal{K}_z}}{\text{minimize}} \quad & \left\{ \sum_{i=1}^{N} \max(1 - C_i/D_i, 0), B, \right. \\
& \left. \sum_{l \in \mathcal{L}} p_l + \sum_{K_z \in \mathcal{K}} \sum_{k \in \mathcal{K}_z} \|\hat{\mathbf{w}}_{k,z}[z]\|_2^2 \right\} \\
\text{s.t.} \quad & L1 : \gamma_i \geq \gamma^{\min}, \forall_i, \\
& L2 : \sum_{l \in \mathcal{L}} p_l + \sum_{K_z \in \mathcal{K}} \sum_{k \in \mathcal{K}_z} \|\hat{\mathbf{w}}_{k,z}[z]\|_2^2 \leq P_{\text{total}}, \\
& L3 : p_l \leq P_{\max}, \forall_l, \\
& L4 : \|\hat{\mathbf{w}}_{k,z}[z]\|_2^2 \leq P_{\max}, \forall_k \in \mathcal{K}_z,
\end{aligned}
$$

2. Note that, in practice, full-precoding can be more challenging when there are many beams because of the need to calculate a larger amount of precoding coefficients and the additional signal processing required when precoding coefficients are combined with symbols for transmission [51]. Hence, partial-precoding can be applied to alleviate the above problems associated with full-precoding.

$$
\begin{aligned}
& L5 : B \leq B_{\text{total}}, \\
& L6 : B \geq B_c \\
& L7 : p_l \geq 0, \forall_l, \quad (7)
\end{aligned}
$$

Objective function in (7) contains the system bandwidth utilization, total power consumption, and unmet system capacity. The constraint $L1$ imposes the minimum SINR required for all beams. The constraint $L2$ prohibits the overall power allocation from exceeding the total system power. Similarly, $L3$ and $L4$ are the per beam power allocation and limits the maximum beam power. Constraint $L5$ and $L6$ are the upper bound and lower bound limits of B, where B_c is the minimum bandwidth requirement by the system. Moreover, $L7$ is a non-negative power constraint.

To reformulate the problem (7) into a more tractable one, we make the following modifications

- Firstly, we convert the multi-objective optimization to a single objective optimization [52] by summing up the normalized object functions, i.e., $\frac{B}{B_{\text{total}}} + \sum_{l \in \mathcal{L}} \frac{p_l}{P_{\text{total}}} + \sum_{K_z \in \mathcal{K}} \sum_{k \in \mathcal{K}_z} \frac{\|\hat{\mathbf{w}}_{k,z}[z]\|_2^2}{P_{\text{total}}} + \sum_{i=1}^{N} \max(1 - C_i/D_i, 0)$.
- Secondly, we avoid the non-differential function using upper bound slack variable φ_i, with $\varphi_i \geq 0, \forall_i$ and $\varphi_i \geq 1 - C_i/D_i, \forall_i$.
- Then, we replace both bandwidth and slack variable φ_i using equivalent representation. The bandwidth is replaced by $T = \frac{1}{B}$ and the variable φ_i is replaced by unmet spectral efficiency $s_i = T\varphi_i$. This variables change will help us to decouple the bandwidth from the capacity.
- Thirdly, we replace the transmit power by Power Spectral Density (PSD), i.e., $\widetilde{p}_l = Tp_l$ and $\widetilde{\mathbf{w}}_{k,z}[z] = \sqrt{T}\hat{\mathbf{w}}_{k,z}[z]$.
- Then, the SINR in terms of PSD is given by

$$
\gamma_l = \frac{g_{l,l}\widetilde{p}_l}{\sum_{j \in \mathcal{L}, j \neq l} g_{l,j}\widetilde{p}_j + \sum_{K_z \in \mathcal{K}} \sum_{j \in \mathcal{K}_z} \left|\hat{\mathbf{h}}_{l,z}^H[z]\widetilde{\mathbf{w}}_{j,z}[z]\right|^2 + N_0} \quad (8)
$$

and

$$
\gamma_{k,m} = \frac{\left|\hat{\mathbf{h}}_{k,m}^H[m]\widetilde{\mathbf{w}}_{k,m}[m]\right|^2}{\sum_{K_z \in \mathcal{K}} \sum_{j \in \mathcal{K}_z, j \neq k} \left|\hat{\mathbf{h}}_{k,m}^H[z]\widetilde{\mathbf{w}}_{j,m}[z]\right|^2 + \sum_{l \in \mathcal{L}} g_{k,l}\widetilde{p}_l + N_0}. \quad (9)
$$

Hence, we make the SINR only dependent on PSD. Consequently, we express the capacity in terms of PSD.

- Finally, we express $L2$, $L3$ and $L4$ in terms of PSD and bandwidth: $\sum_{l \in \mathcal{L}} \widetilde{p}_l + \sum_{K_z \in \mathcal{K}} \sum_{k \in \mathcal{K}_z} \|\widetilde{\mathbf{w}}_{k,z}[z]\|_2^2 \leq TP_{\text{total}}$, $\widetilde{p}_l \leq TP_{\max}, \forall_l$, and $\|\widetilde{\mathbf{w}}_{k,z}[z]\|_2^2 \leq TP_{\max}, \forall_k \in \mathcal{K}_z$, respectively. Similarly, the constraint $L7$ in terms of PSD is $\widetilde{p}_l \geq 0, \forall_l$.

With the above-listed modifications, the equivalent of (7) is given by

$$
\begin{aligned}
& \underset{\substack{T, s_i, \widetilde{p}_l, \forall_l, \\ \widetilde{\mathbf{w}}_{k,z}[z], \forall_k \in \mathcal{K}_z}}{\text{minimize}} \quad \frac{\sum_{i=1}^N s_i + \frac{1}{B_{\text{total}}} + \frac{1}{P_{\text{total}}}\Big(\sum_{l \in \mathcal{L}} \widetilde{p}_l + \sum_{K_z \in \mathcal{K}} \sum_{k \in \mathcal{K}_z} \|\widetilde{\mathbf{w}}_{k,z}[z]\|_2^2\Big)}{T}
\end{aligned}
$$

$$
\text{s.t.} \quad \hat{L}1 : \gamma_i \geq \gamma^{\min}, \forall_i,
$$
$$
\hat{L}2 : \sum_{l \in \mathcal{L}} \widetilde{p}_l + \sum_{K_z \in \mathcal{K}} \sum_{k \in \mathcal{K}_z} \|\widetilde{\mathbf{w}}_{k,z}[z]\|_2^2 \leq TP_{\text{total}},
$$
$$
\hat{L}3 : \widetilde{p}_l \leq TP_{\max}, \forall_l,
$$
$$
\hat{L}4 : \|\widetilde{\mathbf{w}}_{k,z}[z]\|_2^2 \leq TP_{\max}, \forall_k \in \mathcal{K}_z,
$$
$$
\hat{L}5 : 1 \leq TB_{\text{total}},
$$
$$
\hat{L}6 : 1 \geq TB_c,
$$
$$
\hat{L}7 : \widetilde{p}_l \geq 0, \forall_l,
$$
$$
\hat{L}8 : T - \frac{\log_2(1 + \gamma_i)}{D_i} \leq s_i, \forall_i,
$$
$$
\hat{L}9 : s_i \geq 0, \forall_i. \tag{10}
$$

The non-linearity of objective function and γ_i make (10) non-convex. We apply Dinkelbach method [53] to linearize the objective function. Then, the equivalent linear function is given by $1 + \frac{B_{\text{total}}}{P_{\text{total}}}(\sum_{l \in \mathcal{L}} q_l^2 + \sum_{K_z \in \mathcal{K}} \sum_{k \in \mathcal{K}_z} \|\widetilde{\mathbf{w}}_{k,z}[z]\|_2^2) + B_{\text{total}} \sum_{i=1}^N s_i - \beta B_{\text{total}} T$, where β is obtained using Dinkelbach's algorithm. However, the non-convexity of γ_i prevents form directly applying of Dinkelbach method. Hence, convexification of γ_i is required. To convexify γ_i, first, we decouple γ_i from the rate capacity using a lower bound slack variable Γ_i as follows

$$
\hat{L}8.1 : T - \frac{\log_2(1 + \Gamma_i)}{D_i} \leq s_i, \forall_i,
$$

$$
\hat{L}8.2 : \Gamma_i \leq \begin{cases} \gamma_l, & \text{if } i = l, l \in \mathcal{L} \\ \gamma_{k,m} & \text{if } i = k, k \in \mathcal{K}_z, \end{cases} \tag{11}
$$

The constraint $\hat{L}8.1$ is convex. However, $\hat{L}8.2$ is non-convex. By replacing γ_l and $\gamma_{k,m}$, respectively, with (8) and (9), then re-arranging $\hat{L}8.2$, we obtain

$$
\hat{L}8.2 : \begin{cases} \dfrac{\sum_{K_z \in \mathcal{K}} \sum_{j \in \mathcal{K}_z} \left|\hat{\mathbf{h}}_{l,z}^H[z] \widetilde{\mathbf{w}}_{j,z}[z]\right|^2 +}{\sum_{j \in \mathcal{L}, j \neq l} g_{l,j} q_j^2 + N_0 - \frac{g_{l,l} q_l^2}{\Gamma_i}} \leq 0, & \text{if } i = l \\[4ex] \dfrac{\sum_{K_z \in \mathcal{K}} \sum_{j \in \mathcal{K}_z, j \neq k} \left|\hat{\mathbf{h}}_{k,m}^H[z] \widetilde{\mathbf{w}}_{j,m}[z]\right|^2 +}{\sum_{l \in \mathcal{L}} g_{k,l} q_l^2 + N_0 - \frac{\left|\hat{\mathbf{h}}_{k,m}^H[m] \widetilde{\mathbf{w}}_{k,m}[m]\right|^2}{\Gamma_i}} \leq 0, & \text{if } i = k, \end{cases} \tag{12}
$$

where $q_l = \sqrt{\widetilde{p}_l}, \forall_l$. The function $\frac{g_{l,l} q_l^2}{\Gamma_i}$ and $\frac{|\hat{\mathbf{h}}_{k,m}^H[m] \widetilde{\mathbf{w}}_{k,m}[m]|^2}{\Gamma_i}$ as well as the interference signal functions are convex functions [54]. Therefore, $\hat{L}8.2$ is arranged in the form of Difference-of-Convex program (DC). The DC program can be tackled using Successive Convex Approximation (SCA)[3] algorithm (cf. [56]) by approximating the concave part of $\hat{L}8.2$. The SCA of $\hat{L}8.2$ is given by (13), shown at the bottom of the page and $\widetilde{\mathbf{w}}_{k,m}[m]^{(v)}$ and $q_l^{(v)}$ are the previous value of $\widetilde{\mathbf{w}}_{k,m}[m]$ and q_l, respectively. Note that the first-order approximation is rearranged to be evaluated at a single point (i.e., the previous value of the power variable) rather than two points (i.e., the previous values of the power and SINR variables). Thus, the computation time and the number of feasible points for initializing the problem are reduced.

The detail derivation of (13) is provided in Appendix A. Hence, the convexified optimization problem is written as

$$
\underset{\substack{T, s_i, \forall_i, q_l, \forall_l, \\ \widetilde{\mathbf{w}}_{k,z}[z], \forall_k \in \mathcal{K}_z}}{\text{minimize}} \quad \begin{aligned} & 1 + B_{\text{total}} \sum_{i=1}^N s_i - \beta B_{\text{total}} T + \\ & \frac{B_{\text{total}}}{P_{\text{total}}}\Big(\sum_{l \in \mathcal{L}} q_l^2 + \sum_{K_z \in \mathcal{K}} \sum_{k \in \mathcal{K}_z} \|\widetilde{\mathbf{w}}_{k,z}[z]\|_2^2\Big) \end{aligned}
$$

3. A proof of convergence of this SCA approximation has been studied in [55].

$$
\hat{L}8.3 : \Gamma_i \leq \begin{cases} \dfrac{2 g_{l,l} q_l^{(v)} q_l}{I_l^{(v)}} - \dfrac{g_{l,l}\left(q_l^{(v)}\right)^2 I_l}{\left(I_l^{(v)}\right)^2} & \text{if } i = l \\[4ex] \dfrac{2\Re\left\{\left(\widetilde{\mathbf{w}}_{k,m}^{(v)}[m]\right)^H \hat{\mathbf{h}}_{k,m}[m] \hat{\mathbf{h}}_{k,m}^H[m] \widetilde{\mathbf{w}}_{k,m}[m]\right\}}{I_{k,m}^{(v)}} - \dfrac{\left|\hat{\mathbf{h}}_{k,m}^H[m]\left(\widetilde{\mathbf{w}}_{k,m}^{(v)}[m]\right)^H\right|^2 I_{k,m}}{\left(I_{k,m}^{(v)}\right)^2} & \text{if } i = k \end{cases} \tag{13}
$$

with

$$
I_l = \sum_{j \in \mathcal{L}, j \neq l} g_{l,j} q_j^2 + \sum_{K_z \in \mathcal{K}} \sum_{j \in \mathcal{K}_z} \left|\hat{\mathbf{h}}_{l,z}^H[z] \widetilde{\mathbf{w}}_{j,z}[z]\right|^2 + N_0 \tag{14}
$$

$$
I_l^{(v)} = \sum_{j \in \mathcal{L}, j \neq l} g_{l,j}\left(q_j^{(v)}\right)^2 + \sum_{K_z \in \mathcal{K}} \sum_{j \in \mathcal{K}_z} \left|\hat{\mathbf{h}}_{l,z}^H[z] \widetilde{\mathbf{w}}_{j,z}^{(v)}[z]\right|^2 + N_0 \tag{15}
$$

$$
I_{k,m} = \sum_{K_z \in \mathcal{K}} \sum_{j \in \mathcal{K}_z, j \neq k} \left|\hat{\mathbf{h}}_{k,m}^H[z] \widetilde{\mathbf{w}}_{j,m}[z]\right|^2 + \sum_{l \in \mathcal{L}} g_{k,l} q_l^2 + N_0 \tag{16}
$$

$$
I_{k,m}^{(v)} = \sum_{K_z \in \mathcal{K}} \sum_{j \in \mathcal{K}_z, j \neq k} \left|\hat{\mathbf{h}}_{k,m}^H[z] \widetilde{\mathbf{w}}_{j,m}^{(v)}[z]\right|^2 + \sum_{l \in \mathcal{L}} g_{k,l}\left(q_l^{(v)}\right)^2 + N_0 \tag{17}
$$

$$\text{s.t.} \quad \hat{L}1 : \Gamma_i \geq \gamma^{\min}, \forall_i,$$
$$\hat{L}2 : \sum_{l \in \mathcal{L}} q_l^2 + \sum_{K_z \in \mathcal{K}} \sum_{k \in \mathcal{K}_z} \|\widetilde{\mathbf{w}}_{k,z}[z]\|_2^2 \leq TP_{\text{total}},$$
$$\hat{L}3 : q_l^2 \leq TP_{\max}, \forall_l,$$
$$\hat{L}4, \hat{L}5, \hat{L}6, \hat{L}7, \hat{L}8.1, \hat{L}8.3, \hat{L}9. \tag{18}$$

Problem (18) is convex and can be solved efficiently using convex optimization tools [57]. In the following a solution to this problem will be presented.

A. SELECTION OF BEAMS TO BE PRECODED

We select K-beams to be precoded from N beams based on the characteristics of demand, the interference and the channel gain of the user. For this, we use a user-satisfaction metric and interference-to-noise metric. For the selection of beams, we initially assume that the system employs B_{total} and equal power, i.e., $p_i = \frac{P_{\text{total}}}{N}$ for all users, then the user-satisfaction metric for the user in beam i is given by

$$\text{US}_i = \frac{B_{\text{total}} \log_2(1 + \gamma_i^{\text{US}})}{D_i} \tag{19}$$

with

$$\gamma_i^{\text{US}} = \frac{g_{i,i} p_i}{\sum_{j=1, j \neq i}^N g_{i,j} p_j + N_0 B_{\text{total}}}. \tag{20}$$

The interference-to-noise metric for user in beam i from beam j is defined as $\text{I/N}_{i,j} = \frac{g_{i,j} p_j}{N_0 B_{\text{total}}}$. We denote the set that contain the user-satisfaction metric of all users as $\mathcal{S} = \{\text{US}_i, \text{US}_2, \ldots, \text{US}_i, \ldots, \text{US}_N\}$. Similarly, we denote the set that contain the interference-to-noise metric for user in beam i from all other beams as $\mathcal{I}_i = \{\text{I/N}_{i,j}, \forall_{j \neq i}\}$.

The proposed algorithm to select beams for precoding is shown in Algorithm 1. First, we collect beams that do not satisfy the minimum user-satisfaction metric threshold value of ϵ_1, i.e., $US_i < \epsilon_1$ into set $\mathcal{G}$. Then, in the nth iteration, the algorithm selects beam i that has lowest user-satisfaction from $\mathcal{G}$ and we collect it in the set $\mathcal{K}_n$. Subsequently, the algorithm includes beams into set $\mathcal{K}_n$ from $\mathcal{I}_i$ that satisfied the minimum interference-to-noise metric threshold value of ϵ_2. Consequently, the algorithm removes any beam element of $\mathcal{K}_n$ that is present in $\mathcal{G}$ and $\mathcal{I}_i, \forall_i$, i.e., $\mathcal{G} \leftarrow \mathcal{G} \setminus \mathcal{K}_n$ and $\mathcal{I}_i \leftarrow \mathcal{I}_i \setminus \mathcal{K}_n, \forall_i$, respectively. For the $n + 1$ iteration, it continues to select the next beam j that has lowest user-satisfaction from $\mathcal{G}$ and the corresponding beams $\mathcal{I}_j$. The algorithm runs until $|\mathcal{G}|$ becomes empty. Fig. 2 shows an example of partial precoding for $\epsilon_1 = 1$ and $\epsilon_2 = -11$dB, where the colored beams are the selected beam for precoding.

Finally, the iterative procedure to solve (18) is shown in Algorithm 2. First, we initialize $q_l^{(v)}$ and β to a feasible point (See Section III-B). Then, Algorithm 1 is executed in order to select the beams to be jointly precoded. Accordingly, the algorithm solves (18). Subsequently, we update the old value of $q_l^{(v)}$, $\widetilde{\mathbf{w}}_{k,z}^{(v)}[z]$, and β by the new value q_l, $\widetilde{\mathbf{w}}_{k,z}[z]$,
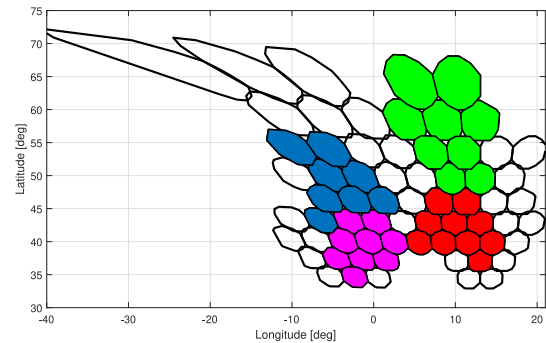

FIGURE 2. Partial precoding with $\epsilon_1 = 1$ and $\epsilon_2 = -11$dB.

Algorithm 1: K-Beam Selection

Input: $\mathcal{S}$; $\mathcal{I}_i, \forall_i$;
$\mathcal{G} \leftarrow$ All beams with $\mathcal{S} < \epsilon_1$;
$n \leftarrow 0$;
while $|\mathcal{G}| \geq 0$ **do**
  $n \leftarrow n + 1$;
  $\mathcal{K}_n \leftarrow \min\{\mathcal{G}\}$;
  $\mathcal{M} \leftarrow$ All beams with $\mathcal{I}_i \geq \epsilon_2$;
  $\mathcal{K}_n \leftarrow \{\mathcal{M} \cup \mathcal{K}_n\}$;
  $\mathcal{G} \leftarrow \mathcal{G} \setminus \mathcal{K}_n$;
  $\mathcal{I}_i \leftarrow \mathcal{I}_i \setminus \mathcal{K}_n, \forall_i$

Algorithm 2: Resource Optimization With Partial Precoding

Input: feasible point $\widetilde{\mathbf{w}}_{k,z}^{(v)}[z]$, $q_l^{(v)}$; β;
$v \leftarrow 0$;
Execute **Algorithm 1**;
repeat
  $v \leftarrow v + 1$;
  Solve (18) to obtain $\widetilde{\mathbf{w}}_{k,z}[z]$, q_l ;
  Update $q_l^{(v)} = q_l$;
  Update $\widetilde{\mathbf{w}}_{k,z}^{(v)}[z] = \widetilde{\mathbf{w}}_{k,z}[z]$;
  Update
  $\beta = \frac{\sum_{i=1}^N s_i + \frac{1}{B_{\text{total}}} + \frac{1}{P_{\text{total}}} \left(\sum_{l \in \mathcal{L}} q_l^2 + \sum_{K_z \in \mathcal{K}} \sum_{k \in \mathcal{K}_z} \|\widetilde{\mathbf{w}}_{k,z}[z]\|_2^2 \right)}{T}$;
until $\{J_1, J_2, \text{ and } J_3\}$;
Output: $B = \frac{1}{T}$;
Output: $\hat{\mathbf{w}}_{k,z}[z] = \sqrt{B} \widetilde{\mathbf{w}}_{k,z}^{(v)}[z], \forall_k \in \mathcal{K}_z$;
Output: $p_l = B(q_l^{(v)})^2, \forall_l$;

---

and $\frac{\frac{1}{B_{\text{total}}} + \frac{1}{P_{\text{total}}} (\sum_{l \in \mathcal{L}} q_l^2 + \sum_{K_z \in \mathcal{K}} \sum_{k \in \mathcal{K}_z} \|\widetilde{\mathbf{w}}_{k,z}[z]\|_2^2) + \sum_{i=1}^N s_i}{T}$, respectively. Note that Algorithm 2 is designed to execute the Dinkelbatch method and SCA at the same time rather than considering Dinkelbatch method as main loop and SCA as inner loop such that the computational time is reduced. The algorithm is run until the convergence criteria J_1, J_2, and J_3 of (21), shown at the bottom of the next page are met. Note

that in the convergence point, we obtain:

$$\Gamma_l \approx \frac{g_{l,l}\left(q_l^{(v)}\right)^2}{\sum_{j\in\mathcal{L},j\neq l} g_{l,j}\left(q_j^{(v)}\right)^2 +}, \forall l$$

$$\sum_{K_z\in\mathcal{K}}\sum_{j\in\mathcal{K}_z}\left|\hat{\mathbf{h}}_{l,z}^H[z]\widetilde{\mathbf{w}}_{j,z}^{(v)}[z]\right|^2 + N_0$$

$$\Gamma_{k,m} \approx \frac{\left|\hat{\mathbf{h}}_{k,m}^H[m]\widetilde{\mathbf{w}}_{k,m}^{(v)}[m]\right|^2}{\sum_{K_z\in\mathcal{K}}\sum_{j\in\mathcal{K}_z,j\neq k}\left|\hat{\mathbf{h}}_{k,m}^H[z]\widetilde{\mathbf{w}}_{j,m}^{(v)}[z]\right|^2 +}, \forall k$$

$$\sum_{l\in\mathcal{L}} g_{k,l}\left(q_l^{(v)}\right)^2 + N_0$$

$$1 + B_{\text{total}}\sum_{i=1}^{N} s_i - \beta B_{\text{total}}T+$$

$$\frac{B_{\text{total}}}{P_{\text{total}}}\left(\sum_{l\in\mathcal{L}}\left(q^{(v)}\right)_l^2 + \sum_{K_z\in\mathcal{K}}\sum_{k\in\mathcal{K}_z}\|\widetilde{\mathbf{w}}_{k,z}^{(\mathbf{v})}[z]\|_2^2\right) \approx 0.$$

B. FEASIBLE POINT INITIALIZATION FOR THE PROPOSED TECHNIQUE

A feasible point initialization is required for the stability of the algorithm execution. For this, we observe that the feasible point for Algorithm 2 is obtained when all non-precoder users equally share the total available power sepectral density, i.e., $(q_l^{(v)})^2 = (\frac{P}{B_{\text{total}}})$, where $P = \frac{P_{\text{total}}}{N}$. Further, to initialize the precoder matrix of Algorithm 2, we start with the MMSE precoder. The MMSE precoder matrix is given by

$$\widetilde{\mathbf{W}}_m = \eta\frac{\hat{\mathbf{W}}_m}{\sqrt{B_{\text{total}}}}, \tag{22}$$

with

$$\hat{\mathbf{W}}_m = \hat{\mathbf{H}}^H\left(\hat{\mathbf{H}}_m\hat{\mathbf{H}}_m^H + \alpha I\right)^{-1}, \tag{23}$$

$$\eta = \sqrt{\frac{P|\mathcal{K}_m|}{\text{Trace}\{\hat{\mathbf{W}}_m\hat{\mathbf{W}}_m^H\}}} \tag{24}$$

where α is the regularization factor given by $\alpha = \frac{N_0 B_{\text{total}}}{P}$. Then, for $s_i=0$ using J_3, the feasible point[4] for β approximately becomes 2.

---

4. Note that for equal power per user with full bandwidth utilization B_{total}, the function $\frac{B_{\text{total}}}{P_{\text{total}}}(\sum_{l\in\mathcal{L}}(q^{(v)})_l^2 + \sum_{K_z\in\mathcal{K}}\sum_{k\in\mathcal{K}_z}\|\widetilde{\mathbf{w}}_{k,z}^{(\mathbf{v})}[z]\|_2^2)$ becomes 1. Then, $J3$ is reduced to $|1 + 1 - \beta| \leq 10^{-4}$. Hence, the approximate value of β is 2.

C. COMPLEXITY ANALYSIS

The complexity of Algorithm 2 is given by $F(v)Q(L,K)$, where the complexity function $F(v)$ indicates the number of iterations required Algorithm 2 to complete and the complexity function $Q(L,K)$ refers to solving (18) which depends on the number of beams L and K. Note that the algorithm requires at most $F(v) = 25$ iterations to complete. Hence, the overall complexity[5] is shown as follows

1) Partial precoding: the problem (18) have $(N+L+K^2+1)$ decision variables and $5N+3$ convex constraints. Then, the complexity function $Q(L,K)$ is $\mathcal{O}((N+L+K^2+1)^3(5N+3))$ [34]. Assuming that V_{pp} iterations are needed for Algorithm 2 to converge, i.e., $F(v) = V_{pp}$, then the overall complexity is $\mathcal{O}(V_{pp}(N+L+K^2+1)^3(5N+3))$.

2) Full-precoding: In this case, the (18) will have $(N+N^2+1)$ decision variables and $5N+3$ convex constraints. Assuming that V_{fp} iterations are needed for Algorithm 2 to converge, i.e., $F(v) = V_{fp}$, then the overall complexity is $\mathcal{O}(V_{fp}(N+N^2+1)^3(5N+3))$.

3) Without precoding: Here (18) will have $(2N+1)$ decision variables and $5N+3$ convex constraints. Assuming that V_{wp} iterations are needed for the Algorithm 2 to converge, i.e., $F(v) = V_{wp}$, then the overall complexity is $\mathcal{O}(V_{wp}(2N+1)^3(5N+3))$.

IV. SIMULATION RESULTS

In this section, we evaluate the performance of the proposed technique in three scenarios, i.e., for a system without precoding, with full precoding, and partial precoding. Table 2 shows the simulation parameters. We consider the user location data for $N = 67$ beams according to [58]. The data contains population, aeronautical, and maritime users. The beam pattern is provided by the European Space Agency (ESA) and generated assuming a Direct Radiating Antenna (DRA), with 750 elements spaced by 5λ. Furthermore, we average all the simulation results for 100 Monte-Carlo runs. For each run, a random user location per beam is selected from the user location data. An example of user locations for a single run is shown in Fig. 3.

---

5. Note that Algorithm 1 is excluded in the computational complexity analysis because its impact is less than the loop in the Algorithm 2.

$$J_1 : \sum_l \left|\frac{g_{l,l}q_l^{(v)}q_l}{I_l^{(v)}} - \frac{g_{l,l}\left(q_l^{(v)}\right)^2 I_l}{\left(I_l^{(v)}\right)^2}\right| \leq 10^{-4}$$

$$J_2 : \sum_{K_m\in\mathcal{K}}\sum_{k\in\mathcal{K}_m}\left|\frac{\Re\left\{\left(\widetilde{\mathbf{w}}_{k,m}^{(v)}[m]\right)^H\hat{\mathbf{h}}_{k,m}[m]\hat{\mathbf{h}}_{k,m}^H[m]\widetilde{\mathbf{w}}_{k,m}[m]\right\}}{I_{k,m}^{(m)}} - \frac{\left|\hat{\mathbf{h}}_k^H\left(\widetilde{\mathbf{w}}_{k,m}[m]^{(v)}\right)^H\right|^2 I_{k,m}}{\left(I_{k,m}^{(v)}\right)^2}\right| \leq 10^{-4}$$

$$J_3 : \left|1 + \frac{B_{\text{total}}}{P_{\text{total}}}\left(\sum_{l\in\mathcal{L}}q_l^2 + \sum_{K_z\in\mathcal{K}}\sum_{k\in\mathcal{K}_z}\|\widetilde{\mathbf{w}}_{k,z}[z]\|_2^2\right) + B_{\text{total}}\sum_{i=1}^{N} s_i - \beta B_{\text{total}}T\right| \leq 10^{-4} \tag{21}$$

TABLE 2. System parameters.

Parameter	Value
Satellite Orbit	13°E
Satellite Beam Pattern	Provided by ESA
Number of beams (N)	67
System bandwidth (B_{total})	500 MHz
Minimum SINR ($\gamma^{\min}$)	-2.2 dB
Minimum bandwidth (B_C)	5 MHz
Noise power density (N_0)	-204 dBW/Hz
Max. beam gain ($G_i[j]$)	51.8 dBi
User antenna gain (G_R)	39.8 dBi
Total available transmit power (P_{total})	1000W
Maximum power per beam ($P_{\max}$)	100W
User-satisfaction metric threshold	$\epsilon_1 = 1$
Interference-to-noise metric threshold	$\epsilon_2 = -11$dB
Percentage ($\mathcal{P}$)	1%

FIGURE 5. The average normalized demand per beam.

FIGURE 6. The low-moderate demand and the moderate-high demand distribution.
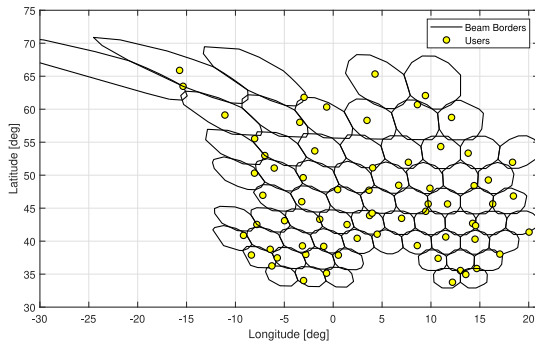

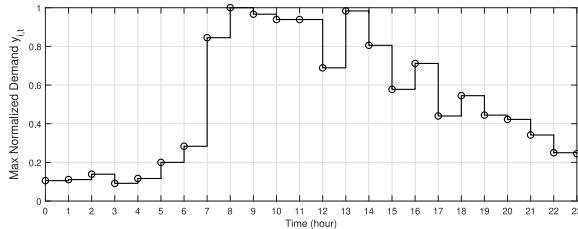**FIGURE 3.** User distribution for $N = 67$ beam.

FIGURE 4. The average hourly demand request.

We consider the performance indicators: Average Unmet System Capacity (AUSC), Average utilized Bandwidth (AUB), and the Average Power Consumption (APC) [34]. Additionally, we define the Total Resource Utilization (TRU) in percent as

$$\text{TRU} = \frac{100}{2}\left(\frac{\text{APC}}{P_{\text{total}}} + \frac{\text{AUB}}{B_{\text{total}}}\right)\%. \quad (25)$$

1) TRAFFIC MODEL

In this section, we generate a traffic demand for the simulation results using the normalized temporal and spatial demand distributions, which are shown in Figs. 4 and 5, respectively. These demand distributions are adopted from the traffic simulator provided in [58]. The temporal distribution represents the average demand per beam at a given time t divided by the peak demand average request $D^{\max} = 7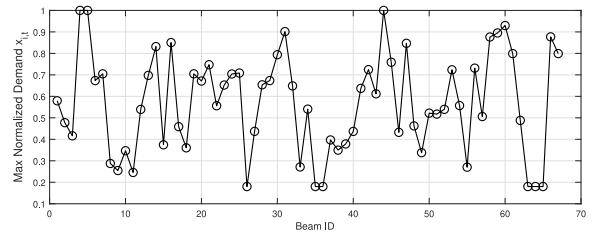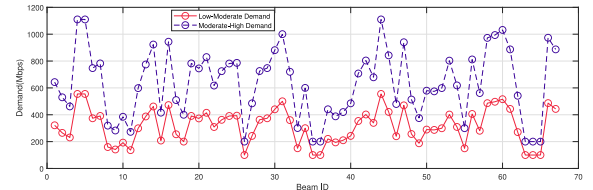50$ Mbps. Accordingly, we can calculate the average demand at t hour as $D_t^{\text{avg}} = y_{i,t} D^{\max}$, where $y_{i,t}$ represents the normalized demand at time t. For example, the average demand per beam at $t = 7$ with $y_{i,7} = 0.844906750$ and $t = 20$ with $y_{i,20} = 0.422453750$ is $D_7^{\text{avg}} = 634$ Mbps and $D_{20}^{\text{avg}} = 317$ Mbps, respectively.

The spatial distribution in Fig. 5 represents the demand per beam normalized by the maximum beam demand $D_{s,t}^{\max}$. The $D_{s,t}^{\max}$ is obtained from temporal distribution as $D_{s,t}^{\max} = \frac{N D_t^{\text{avg}}}{\sum_{i=1}^{N} x_i}$ Mbps, where x_i is the spatial normalized demand of beam i. For example, at $t = 7$ and $t = 20$, we obtain $D_{s,7}^{\max} = 1110$ Mbps and $D_{s,20}^{\max} = 555$ Mbps, respectively. Hence, the ith beam demand is given by $D_i = D_{s,t}^{\max} x_i$. Note that each beam represents the sum of population, aeronautical, and maritime demands. Hence, the beam demand can vary depending on the population, aeronautical, and maritime size. For example, a beam with more aeronautical and maritime services may have higher demand than a beam with only population-based data.

In the above context, for the simulation results, we consider two different demand distributions at $t = 7$ and $t = 20$ hour, which we call low-moderate and moderate-high demand as shown Fig. 6. Since demand distributions depend on the population, aeronautical, and maritime size, some beams may show little change in demand between time intervals, while others may show significant change. In the case of low variation, the beam contains a higher population demand than aeronautical or maritime demands. On the other hand, in cases of high demand changes, the beam contains more aeronautical demands than population or maritime demands.

2) WITHOUT PRECODING

We start by comparing the proposed method when the system employs no precoding method, i.e., ($|\mathcal{K}| = 0$), with the benchmark schemes [26] and [32]. For this simulation results, we focus on low-moderate demand distribution.
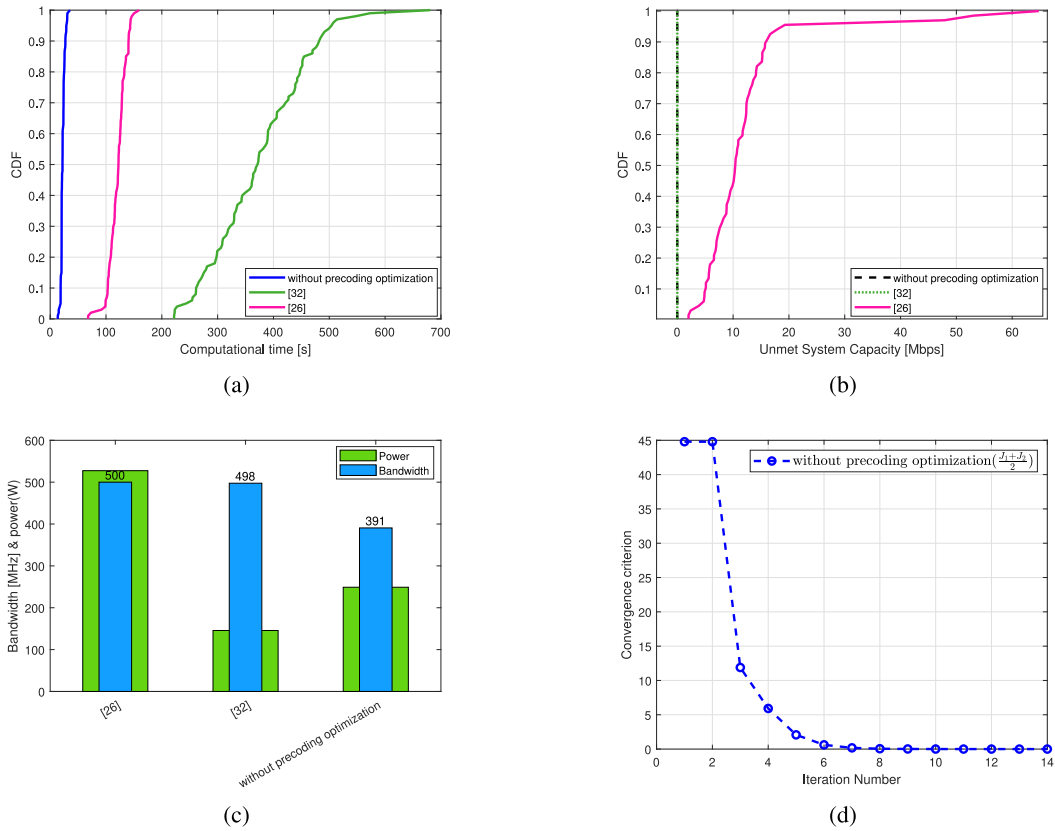
FIGURE 7. Without precoding vs Benchmark schemes for low-moderate demand distribution: (a) Computational time [s]; (b) Unmet System Capacity [Mbps]; (c) Power Consumption [W] and Bandwidth utilization [MHz]; (d) Convergence analysis for without precoding optimization.

Fig. 7a shows the cumulative distribution function (CDF) of the computational time of the proposed without precoding method and the benchmark schemes. We observed that the computational time of the proposed method is lower than the benchmark schemes. For example, at 60% and 100% cases, the proposed method computing time is 22 s and 34 s, respectively, whereas, for [32], the computing time is 390 s and 681 s, respectively. Additionally, the computing time of [26] for 60% and 100% cases is 126 s and 160 s, respectively. This lower computational complexity is achieved because the proposed method is designed to have fewer optimization variables. Consequently, the search space is reduced. In contrast, the benchmark schemes employ a large number of optimization variables. Typically, this leads to higher computational complexity and execution time. For example, the bandwidth B of the proposed method is a single variable, whereas the benchmark schemes assign $\mathcal{Y}$ carrier frequency to N beams from $\mathcal{Y} \times N$ optimization variables.

Fig. 7b shows the CDF of average unmet system capacity for all schemes. We observed that the proposed method and [32] have zero unmet system capacity, whereas the unmet system capacity of [26] is higher than zero. For instance, at 50% and 100% cases, the unmet system capacity of [26] is 10 Mbps and 65 Mbps, respectively. This high unmet system capacity is obtained because [26] employs a metaheuristic method to match the per beam demand. Thus,

the metaheuristic method may not guarantee an optimal solution. In contrast, the proposed method and [32] use approximate convex algorithms that optimize the satellite resource according to the demand. Hence, using the proposed method and [32] results in a lower unmet system capacity.

The resource utilization for the proposed method, [32] and [26] is shown in Fig. 7c. The total resource utilization for the proposed method is 51.6%. In contrast, for [32], the TRU is 57.1% and for [26], the TRU is 76.4%. Hence, the proposed method gives better resource utilization in addition to the substantial savings in computational complexity, as explained before.

Fig. 7d shows the convergence of the proposed Algorithm 2 for $K = 0$. For the convergence analysis, we plot the average of the convergence criteria of J_1 and J_3 for each iteration of Algorithm 2. We observed that the proposed algorithm converged to a stationary point.

3) PARTIAL PRECODING AND FULL-PRECODING

Next, we would like to study the performance of the system with partial precoding ($|\mathcal{K}_m| < N, \forall_m$) and full precoding (if any $|\mathcal{K}_m| = N$) optimization. We consider the following benchmark schemes:
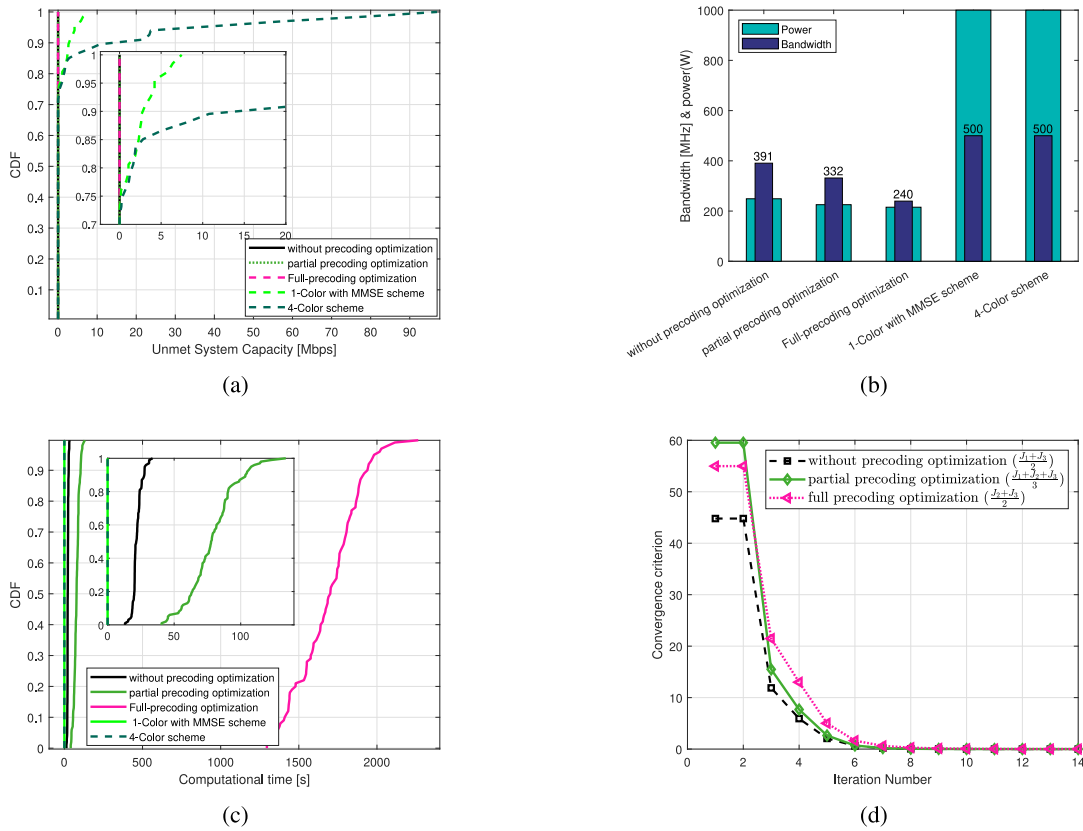
- Without Precoding ($|\mathcal{K}| = 0$)

FIGURE 8. Comparison of the proposed techniques for low-moderate demand distribution: (a) Unmet System Capacity [Mbps]; (b) Power Consumption [W] and Bandwidth utilization [MHz]; (c) Computational time [s]; (d) Convergence analysis.

- 1-Color full bandwidth with MMSE precoder scheme:

$$
C[i] = B_{\text{total}} \log_2 \left(1 + \frac{\left| \mathbf{h}_i^H \mathbf{w}_i \right|^2}{\sum_{\substack{j=1, \\ j \neq i}}^{N} \left| \mathbf{h}_i^H \mathbf{w}_j \right|^2 + N_0 B_{\text{total}}} \right),
$$
(26)

where $\mathbf{w}_i \in \mathbb{C}^{N \times 1}$ is the ith MMSE precoding vector.

- 4-Color scheme without precoding:

$$
C[i] = B_c \log_2 \left(1 + \frac{g_{i,i} a_{k,i} p_i}{\sum_{j=1, j \neq i}^{N} g_{i,j} a_{k,j} p_j + N_0 B_c} \right)
$$
(27)

where $B_c = \frac{B_{\text{total}}}{4}$ is the bandwidth chunk per carrier, $p_i = \frac{P_{\text{total}}}{N}, \forall_i$ is the ith transmitted power and $a_{k,i} \in \{0, 1\}$, $k = 1, 2, 3, 4$ with $a_{k,i} = 1$ indicates that the kth carrier is assigned to the ith beam.

Fig. 8a describes the CDF of the average unmet system capacity of all schemes for low-moderate demand distribution. We observe zero unmet system capacity for all proposed solutions, which indicates 100% demand satisfaction. In contrast, 1-Color with MMSE scheme and 4-Color scheme only satisfy 75% and 71% of the beams, respectively, which indicates that the unmet system capacity is not zero for everyone. This higher unmet system capacity on these schemes results from a lack of resource optimization according to

the demand, where uniform resource allocation is considered. However, the proposed methods without precoding, with partial and full-precoding can allocate resources depending on the demand, which results in lower unmet system capacity. Hence, all proposed methods are suitable for low-moderate demand distribution.

Fig. 8b shows the power consumption and bandwidth utilization of the proposed techniques and the benchmark schemes for low-moderate distribution. The power consumption without precoding, with partial and full-precoding is 249 W, 226 W, and 215 W, respectively, whereas the power consumption for 1-Color with MMSE scheme and 4-Color scheme is 1000 W. Furthermore, the bandwidth utilization of without precoding, partial precoding, and full-precoding is 391 MHz, 326 MHz, and 240 MHz, respectively, whereas the bandwidth utilization for the 1-Color with MMSE scheme and 4-Color scheme is 500 MHz. Hence, we noticed that resource utilization of 1-Color with MMSE scheme and 4-Color scheme is higher than the proposed methods. From the proposed methods, the method without precoding consumes more resources than the partial precoding and full precoding methods. This results from the impact of the interference, which is not entirely canceled and thus affects the signal quality, such that additional signal bandwidth needs to be allocated in order to compensate for this effect. In contrast, we observe lower resource utilization for partial precoding

and full precoding because they can mitigate the interference partially and fully, respectively. Further, the overall utilization using the full precoding is lower compared with the partial precoding optimization. We can verify this result by evaluating the TRU. The TRU is 35% for full precoding, and the TRU is 44% for partial precoding.

Fig. 8c shows the computational time in seconds (s) for all schemes. The computational time of 1-Color with MMSE scheme and 4-Color scheme is in the order of milliseconds which is less than the proposed methods. However, this gain is obtained at the expense of higher unmet system capacity and more resource utilization. From the proposed methods, the method without precoding has less computational time compared with partial and full precoding methods. For instance, for 20% and 100% cases, the computational time required if no precoding is employed is 20 s, and 34 s, respectively. However, with partial precoding and full precoding computational time for 20% is 64 s and 1479 s, respectively, and for 100% cases the computational time for partial precoding and full precoding is 134 s and 2323 s, respectively. This computational time difference results from the size of the optimization variables. For instance, without precoding there are $(2N + 1)$ optimization variables, whereas the partial precoding and full precoding methods have $(N + L + K^2 + 1)$ and $(N + N^2 + 1)$ power optimization variables, respectively, see Section III-C.

The convergence analysis is shown in Fig. 8d. For this, we plot the convergence criteria average of $\{J_1, J_3\}$, $\{J_1, J_2, J_3\}$, and $\{J_2, J_3\}$ for no precoding, partial precoding, and full precoding, respectively. The proposed algorithm converges to a stationary point for all methods.

Generally, in terms of resource utilization efficiency, full-precoding and partial precoding methods provide a better performance compared with the no precoding method. However, the main challenge is that the computational time required to achieve the full precoding and partial precoding is high. Hence, we recommend for low latency, that no precoding is employed, and for limited resource, that the full-precoding method is employed. However, no precoding and full-precoding methods are insufficient in scenarios with strong interference and large number of beams, respectively. While precoding is needed in order to handle the interference, a higher number of beams leads to hardware and time complexity of the system. Therefore, the partial precoding is useful in order to provide trade-off between resource utilization and computational time. Furthermore, it is unlikely that full-precoding can be realized in a practical system since receivers may not be able to estimate all channel coefficients, particularly far-away beams. Additionally, the traffic demand is heterogeneous, with some beams having high demand and others having low demand. Hence, using precoding for low demands may not result in any significant benefits over no precoding; on the contrary, it can add to the system's complexity. In this case, partial precoding is more desirable than full-precoding.
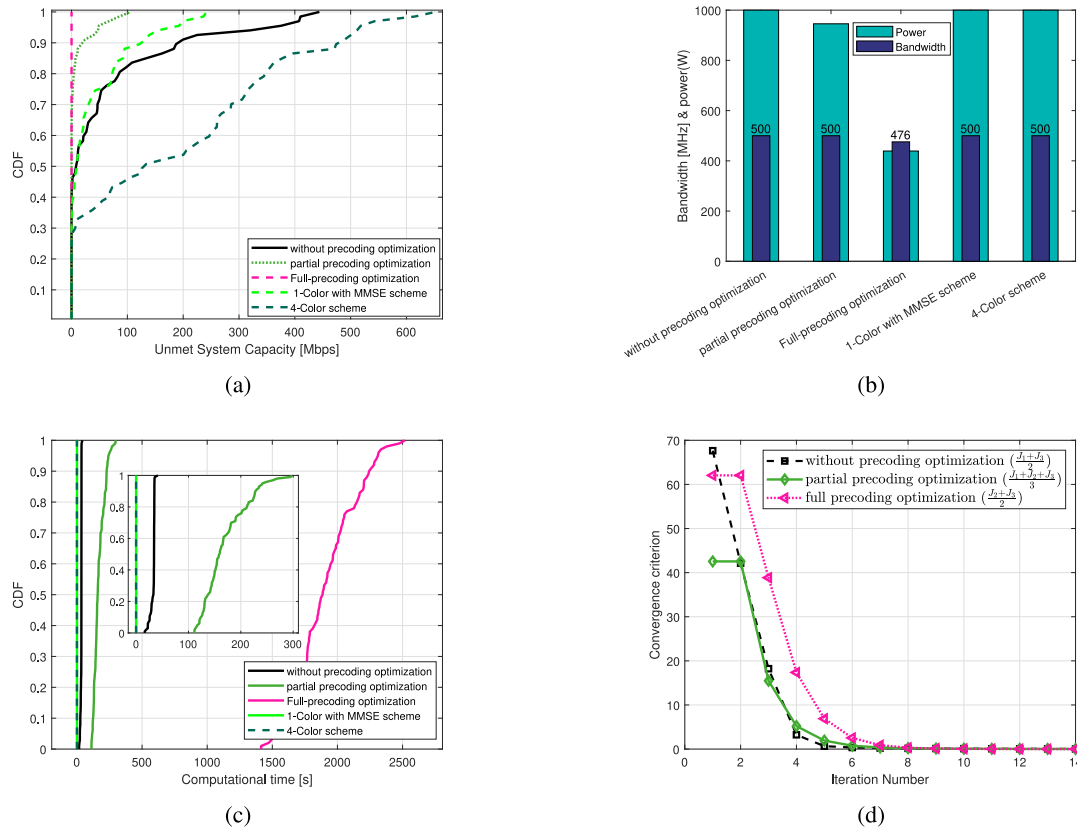
The unmet system capacity of the proposed methods and the benchmark schemes for moderate-high demand distribution is shown in Fig. 9a. For the 1-Color with MMSE scheme, the 4-Color scheme and the no precoding method, 68%, 75%, and 55% of beams, respectively, have non-zero unmet system capacity. Hence, these methods are not suitable for the scenario of high demand satisfaction. In contrast, partial precoding and full precoding have 70% and 100% zero unmet system capacity, respectively, which indicating high demand satisfaction compared with the methods mentioned above. Note that the partial precoding method does not fully mitigate the interference, leading to decreased spectral efficiency. Consequently, some beams have non-zero unmet system capacity.

Fig. 9b shows the resource utilization of the proposed technique and the benchmark schemes for moderate-high demand distribution. The power consumption 1-Color with MMSE scheme, 4-Color scheme, and the proposed without precoding is 1000 W, whereas the power consumption for partial precoding, and full precoding is 946 W, and 439 W, respectively. Additionally, the bandwidth utilization all schemes except the full precoding method is 500 MHz, whereas the bandwidth utilization of full precoding is 476 MHz. We observe the benchmark schemes and without precoding method are fully utilized the system resource. In contrast, partial precoding and full precoding TRU is 97% and 70%, respectively. Like low-demand distribution, we can select the partial precoding method for high-moderate distribution to obtain medium computational time and reasonable demand satisfaction.

Fig. 9c shows the computational time for all schemes. For 100% cases, the computational time of 1-Color with MMSE scheme and 4-Color scheme is five milliseconds. In contrast, the computational time of without precoding, partial precoding and full precoding is 42 s, 295 s, and 2519 s, respectively. The high computational time of the partial precoding, and full precoding is observed because more time is required to determine the value of the decision variables of the optimization problem. However, partial precoding, and full precoding have lower unmet system capacity compared with the benchmark schemes.

Fig. 9d depicts the convergence analysis of the proposed methods. Similar to Fig. 8d, the proposed algorithm converges to a stationary point for the scenario without precoding, partial precoding, and full precoding.

Generally, we observe that the computational time of the proposed algorithm is significantly less than the variability in traffic demand over time. Hence, we can obtain real-time resource allocation from the algorithm to satisfy the traffic demand requests. Accordingly, the digital satellite payload can be configured to dynamically allocate power and bandwidth to each beam depending on its demand. Furthermore, in case the timing becomes a constraint, the solution of proposed method can be used as a starting point for an adaptive algorithm to match the demand variations. This is due to a slow and continuous variation in traffic demand as

FIGURE 9. Comparison of the proposed techniques for moderate-high demand distribution: (a) Unmet System Capacity [Mbps]; (b) Power Consumption [W] and Bandwidth utilization [MHz] ; (c) Computational time [s]; (d) Convergence analysis.

well as communication channels on a satellite-terrestrial link. Hence, the algorithm may not be recomputed each time for a slight change of the parameters. However, this is beyond the scope of this work.

4) RAIN ATTENUATION EFFECT

Here, we examine the performance of the proposed scheme without precoding, partial precoding, and full precoding when the propagation channel is affected by rain attenuation. Hence, we have included the rain attenuation effect in the channel model as follows

$$h_i[j] = \frac{\sqrt{G_R G_i[j]}}{\left(4\pi \frac{d_i}{\lambda}\right)\sqrt{10^{\frac{A_i[\mathcal{P}]}{10}}}} e^{-\jmath \phi_i}, \tag{28}$$

where $A_i[\mathcal{P}][dB]$ is the rain attenuation effect for a user in beam i with a percentage $\mathcal{P}$ of the average rain rate in a year as provided in the Recommendation ITU-R P.618 − 13 [59].

In the following table, we investigate the performance of the proposed scheme when the rain attenuation effect is considered. In the case of low-moderate demand with the rain attenuation effect, the total power and bandwidth consumption without precoding increase on average by 4.4658 W and 0.8789 MHz, respectively, compared to clear sky conditions. This resulted in a 0.32 increase in its TRU. Similarly, the total power consumption of the full-precoding increases by 2.6736 W while the bandwidth consumption

increases by 1.3487 MHz compared to clear sky conditions. Consequently, the TRU increases by 0.27. In the case of partial precoding, the power consumption increases by 3.7686 W while the bandwidth consumption increases by 0.7384 MHz. Accordingly, its TRU increases by 0.26 compared with clear sky conditions. Generally, we observe that the proposed method has zero USC for low-moderate demand and it utilizes more resources to compensate for the rain attenuation effect.

In the case of moderate-high demand, optimization without precoding uses all the resources. However, the unmet system capacity increases by 0.9249 compared to clear sky conditions. In contrast, we observe no change in USC for full-precoding optimization. However, on average, the power and bandwidth consumption of full-precoding increased by 6.7 w and 2.0996 MHz, respectively. Similar to low-moderate demand, the power consumption of partial precoding increases on average by 8.6 W when rain attenuation is considered. Additionally, we also observe the TRU and USC of partial precoding increases by 0.43 and 0.3550 compared with clear sky conditions. In contrast, it utilizes the whole bandwidth.

V. CONCLUSION

In this paper, we propose an advanced radio resource management technique for high throughput GEO satellites. For this, we develop novel algorithms to match the

TABLE 3. Rain attenuation effect.

		Without Precoding				Partial Precoding				Full-precoding			
		Total Power Consumption [W]	Total Bandwidth Consumption [MHz]	TRU [%]	USC	Total Power Consumption [W]	Total Bandwidth Consumption [MHz]	TRU [%]	USC	Total Power Consumption [W]	Total Bandwidth Consumption [MHz]	TRU [%]	USC
Low-moderate Demand	Clear Sky Conditions	248.9671	390.6622	51.51	0	225.4085	331.6915	44.44	0	215.3779	239.5902	34.73	0
	Rain Attenuation	253.4329	391.5411	51.83	0	229.1771	332.4299	44.70	0	218.0515	240.9389	35	0
Moderate-high Demand	Clear Sky Conditions	1000	500	100	40.9272	945.6	500	97.28	4.9730	439.1	475.5549	69.51	0
	Rain Attenuation	1000	500	100	41.8521	954.2	500	97.71	5.3280	445.8	477.6545	70.61	0

demand while minimizing the overall resource utilization. Accordingly, we formulated a multiobjective optimization problem to minimize the system bandwidth utilization, power consumption, and unmet capacity. The nature of the formulated optimization problem is non-convex. Hence, we apply the Dinkelbach method and successive convex approximation to transform the problem into an approximate convex optimization in order to solve it iteratively.

In the above context, we evaluate the system performance with full-precoding, partial precoding, and without precoding. We observe that a system without precoding has a lower computational time. However, because of the interference among the beams, its performance with respect to unmet capacity is high for moderate-high demand distribution. A suitable solution is to mitigate the interference among the beams by employing full-precoding. However, it has high computational time. Finally, we evaluate the system with partial precoding in order to benefit from both lower computational time and lower unmet system capacity. This method shows a promising performance in terms of computational time and overall resource utilization as well as demand satisfaction.

VI. FUTURE WORK

In this work, we developed an efficient algorithm for HTS GEO satellites to provide high-demand satisfaction with appropriate interference mitigation and resource management. With the emerging trends in small satellite deployments in lower orbits, it is a natural step to consider the proposed methodology for non-geostationary orbits. Due to the proximity of these satellites to Earth, the coverage area of a specific satellite is much smaller than that of a GEO satellite, therefore requiring multiple satellites (i.e., a constellation) to provide service in a continuous manner. Hence, a user on the ground is served by one satellite within a few minutes only, and then it switches to another satellite. Accordingly, with appropriate channel characteristics, traffic demand, and satellite constellation information, the proposed algorithm can be applied to each lower orbit satellite to match the user demand and manage the resources while mitigating the interference among satellites and user signals. However, the hand-over across satellites and the subsequent dynamic updating of the resource assignment bring other challenges that need to be further considered in future works. Furthermore, future work will include imperfect channel state information on the channel model to study its effect on resource allocation and demand matching.

APPENDIX A
PROOF SCA OF SECTION III

For $i = l$, the constraint $\hat{L}8.2$ becomes

$$\hat{L}8.2: \begin{array}{c} \sum_{K_z \in \mathcal{K}} \sum_{j \in \mathcal{K}_z} \left| \hat{\mathbf{h}}_{l,z}^H[z] \widetilde{\mathbf{w}}_{j,z}[z] \right|^2 + \\ \sum_{j \in \mathcal{L}, j \neq l} g_{l,j} q_j^2 + N_0 - \frac{g_{l,l} q_l^2}{\Gamma_l} \leq 0 \end{array} \quad (29)$$

Taking the SCA of (29) using first-order approximation is

$$
\begin{aligned}
\hat{L}8.2: & \sum_{K_z \in \mathcal{K}} \sum_{j \in \mathcal{K}_z} \left| \hat{\mathbf{h}}_{l,z}^H[z] \widetilde{\mathbf{w}}_{j,z}[z] \right|^2 \\
& + \sum_{j \in \mathcal{L}, j \neq l} g_{l,j} q_j^2 \\
& + N_0 + \frac{g_{l,l} \left(q_l^{(v)} \right)^2}{\left(\Gamma_l^{(v)} \right)^2} \Gamma_l - 2 \frac{g_{l,l} q_l^{(v)} q_l}{\Gamma_l^{(v)}} \leq 0, \forall l, \quad (30)
\end{aligned}
$$

where $\Gamma_l^{(v)}$ and $q_l^{(v)}$ is the previous value of Γ_l and q_l, respectively. Re-arranging the common terms of (30) leads to

$$
\begin{aligned}
\hat{L}8.2: \Gamma_i \leq & \frac{2\Gamma_l^{(v)} g_{l,l} q_l^{(v)} q_l}{g_{l,l} \left(q_l^{(v)} \right)^2} \\
& - \frac{\left(\Gamma_l^{(v)} \right)^2 \left(\begin{array}{c} \sum_{j \in \mathcal{L}, j \neq l} g_{l,j} q_j^2 + \\ \sum_{K_z \in \mathcal{K}} \sum_{j \in \mathcal{K}_z} \left| \hat{\mathbf{h}}_{l,z}^H[z] \widetilde{\mathbf{w}}_{j,z}[z] \right|^2 + N_0 \end{array} \right)}{g_{l,l} \left(q_l^{(v)} \right)^2}
\end{aligned}
$$
$$(31)$$

Then, we choose that $\Gamma_l^{(v)}$ to be[6]

$$
\Gamma_l^{(v)} = \frac{g_{l,l} \left(q_l^{(v)} \right)^2}{\left(\begin{array}{c} \sum_{j \in \mathcal{L}, j \neq l} g_{l,j} \left(q_j^{(v)} \right)^2 + \\ \sum_{K_z \in \mathcal{K}} \sum_{j \in \mathcal{K}_z} \left| \hat{\mathbf{h}}_{l,z}^H[z] \widetilde{\mathbf{w}}_{j,z}^{(v)}[z] \right|^2 + N_0 \end{array} \right)} .
$$

Then, (31) reduces to

$$\hat{L}8.2: \Gamma_l \leq \frac{2 g_{l,l} q_l^{(v)} q_l}{I_l^{(v)}} - \frac{g_{l,l} \left(q_l^{(v)} \right)^2 I_l}{\left(I_l^{(v)} \right)^2} \quad (32)$$

6. This reduces the computational time as well as the feasible point initialization problem.

with

$$I_l = \sum_{j\in\mathcal{L},j\neq l} g_{l,j}q_j^2 + \sum_{K_z\in\mathcal{K}}\sum_{j\in\mathcal{K}_z}\left|\hat{\mathbf{h}}_{l,z}^H[z]\widetilde{\mathbf{w}}_{j,z}[z]\right|^2 + N_0,$$

$$I_l^{(v)} = \sum_{j\in\mathcal{L},j\neq l} g_{l,j}\left(q_j^{(v)}\right)^2 + \sum_{K_z\in\mathcal{K}}\sum_{j\in\mathcal{K}_z}\left|\hat{\mathbf{h}}_{l,z}^H[z]\widetilde{\mathbf{w}}_{j,z}^{(v)}[z]\right|^2 + N_0.$$

Similarly, for $i = k$ and $m \in \mathcal{K}_m$, the constraint $\hat{L}8.2$ becomes

$$\hat{L}8.2 : \sum_{K_z\in\mathcal{K}}\sum_{j\in\mathcal{K}_z,j\neq k}\left|\hat{\mathbf{h}}_{k,m}^H[z]\widetilde{\mathbf{w}}_{j,m}[z]\right|^2$$
$$+ \sum_{l\in\mathcal{L}} g_{k,l}q_l^2 + N_0 - \frac{\left|\hat{\mathbf{h}}_{k,m}^H[m]\widetilde{\mathbf{w}}_{k,m}[m]\right|^2}{\Gamma_{k,m}} \leq 0. \quad (33)$$

Taking the first order approximation fractional part of (33)

$$\hat{L}8.2 : \sum_{K_z\in\mathcal{K}}\sum_{j\in\mathcal{K}_z,j\neq k}\left|\hat{\mathbf{h}}_{k,m}^H[z]\widetilde{\mathbf{w}}_{j,m}[z]\right|^2$$
$$+ \sum_{l\in\mathcal{L}} g_{k,l}q_l^2 + N_0 - f\left(\widetilde{\mathbf{w}}_{k,m}[m], \Gamma_{k,m}\right) \leq 0, \quad (34)$$

with

$$f\left(\widetilde{\mathbf{w}}_{k,m}[m], \Gamma_{k,m}\right) = \frac{\left|\hat{\mathbf{h}}_{k,m}^H[m]\widetilde{\mathbf{w}}_{k,m}^{(v)}[m]\right|^2}{\Gamma_k^{(v)}}$$

$$- \frac{\left|\hat{\mathbf{h}}_{k,m}^H[m]\widetilde{\mathbf{w}}_{k,m}^{(v)}[m]\right|^2}{\left(\Gamma_{k,m}^{(v)}\right)^2}\left(\Gamma_{k,m} - \Gamma_{k,m}^{(v)}\right)$$

$$+ \frac{2\Re\left\{\left(\widetilde{\mathbf{w}}_{k,m}^{(v)}[m]\right)^H\hat{\mathbf{h}}_{k,m}[m]\hat{\mathbf{h}}_{k,m}^H[m]\left(\widetilde{\mathbf{w}}_{k,m}[m] - \widetilde{\mathbf{w}}_{k,m}^{(v)}[m]\right)\right\}}{\Gamma_{k,m}^{(v)}}.$$

$$(35)$$

Re-arranging the common terms of (34) as follows

$$\Gamma_{k,m} \leq \frac{2\Re\left\{\left(\widetilde{\mathbf{w}}_{k,m}^{(v)}[m]\right)^H\hat{\mathbf{h}}_{k,m}[m]\hat{\mathbf{h}}_{k,m}^H[m]\widetilde{\mathbf{w}}_{k,m}[m]\right\}\Gamma_{k,m}^{(v)}}{\left|\hat{\mathbf{h}}_{k,m}^H[m]\widetilde{\mathbf{w}}_{k,m}^{(v)}[m]\right|^2}$$

$$- \frac{\left(\Gamma_{k,m}^{(v)}\right)^2\left(\sum_{K_z\in\mathcal{K}}\sum_{j\in\mathcal{K}_z,j\neq k}\left|\hat{\mathbf{h}}_{k,m}^H[z]\widetilde{\mathbf{w}}_{j,m}[z]\right|^2 + \sum_{l\in\mathcal{L}} g_{k,l}q_l^2 + N_0\right)}{\left|\hat{\mathbf{h}}_{k,m}^H[m]\widetilde{\mathbf{w}}_{k,m}^{(v)}[m]\right|^2}.$$

$$(36)$$

Then, we choose that $\Gamma_{k,m}^{(v)}$ to be[7]

$$\Gamma_{k,m}^{(v)} = \frac{\left|\hat{\mathbf{h}}_{k,m}^H[m]\widetilde{\mathbf{w}}_{k,m}^{(v)}[m]\right|^2}{\left(\sum_{K_z\in\mathcal{K}}\sum_{j\in\mathcal{K}_z,j\neq k}\left|\hat{\mathbf{h}}_{k,m}^H[z]\widetilde{\mathbf{w}}_{j,m}^{(v)}[z]\right|^2 + \sum_{l\in\mathcal{L}} g_{k,l}\left(q_l^{(v)}\right)^2 + N_0\right)},$$

7. This reduces the computational time as well as the feasible point initialization problem.

then, (36) reduces to

$$\hat{L}8.3 : \Gamma_{k,m} \leq \frac{2\Re\left\{\left(\widetilde{\mathbf{w}}_{k,m}^{(v)}[m]\right)^H\hat{\mathbf{h}}_{k,m}[m]\hat{\mathbf{h}}_{k,m}^H[m]\widetilde{\mathbf{w}}_{k,m}[m]\right\}}{I_{k,m}^{(v)}}$$

$$- \frac{\left|\hat{\mathbf{h}}_{k,m}^H[m]\left(\widetilde{\mathbf{w}}_{k,m}^{(v)}[m]\right)^H\right|^2 I_{k,m}}{\left(I_{k,m}^{(v)}\right)^2}, \quad (37)$$

with

$$I_{k,m} = \sum_{K_z\in\mathcal{K}}\sum_{j\in\mathcal{K}_z,j\neq k}\left|\hat{\mathbf{h}}_{k,m}^H[z]\widetilde{\mathbf{w}}_{j,m}[z]\right|^2 + \sum_{l\in\mathcal{L}} g_{k,l}q_l^2 + N_0,$$

$$I_{k,m}^{(v)} = \sum_{K_z\in\mathcal{K}}\sum_{\substack{j\in\mathcal{K}_z,\\j\neq k}}\left|\hat{\mathbf{h}}_{k,m}^H[z]\widetilde{\mathbf{w}}_{j,m}^{(v)}[z]\right|^2 + \sum_{l\in\mathcal{L}} g_{k,l}\left(q_l^{(v)}\right)^2 + N_0.$$

REFERENCES

[1] T. S. Abdu, S. Kisseleff, E. Lagunas, and S. Chatzinotas, "A low-complexity resource optimization technique for high throughput satellite," in *Proc. 17th Int. Symp. Wireless Commun. Syst. (ISWCS)*, 2021, pp. 1–5.

[2] S. Kisseleff, E. Lagunas, T. S. Abdu, S. Chatzinotas, and B. Ottersten, "Radio resource management techniques for multibeam satellite systems," *IEEE Commun. Lett.*, vol. 25, no. 8, pp. 2448–2452, Aug. 2021.

[3] O. Kodheli *et al.*, "Satellite communications in the new space era: A survey and future challenges," *IEEE Commun. Surveys Tuts.*, vol. 23, no. 1, pp. 70–109, 1st Quart., 2021.

[4] A. I. Perez-Neira, M. A. Vazquez, M. B. Shankar, S. Maleki, and S. Chatzinotas, "Signal processing for high-throughput satellites: Challenges in new interference-limited scenarios," *IEEE Signal Process. Mag.*, vol. 36, no. 4, pp. 112–131, Jul. 2019.

[5] B. Shankar, M. E. Lagunas, S. Chatzinotas, and B. Ottersten, "Precoding for satellite communications: Why, how and what next?" *IEEE Commun. Lett.*, vol. 25, no. 8, pp. 2453–2457, Aug. 2021.

[6] J. P. Choi and V. W. S. Chan, "Optimum power and beam allocation based on traffic demands and channel conditions over satellite downlinks," *IEEE Trans. Wireless Commun.*, vol. 4, no. 6, pp. 2983–2993, Nov. 2005.

[7] N. K. Srivastava and A. K. Chaturvedi, "Flexible and dynamic power allocation in broadband multi-beam satellites," *IEEE Commun. Lett.*, vol. 17, no. 9, pp. 1722–1725, Sep. 2013.

[8] X. P. H. Wang, A. Liu, and J. Li, "Optimization of power allocation for a multibeam satellite communication system with interbeam interference," *J. Appl. Math.*, vol. 2014, Jan. 2014, Art. no. 469437.

[9] A. Destounis and A. D. Panagopoulos, "Dynamic power allocation for broadband multi-beam satellite communication networks," *IEEE Commun. Lett.*, vol. 15, no. 4, pp. 380–382, Apr. 2011.

[10] C. N. Efrem and A. D. Panagopoulos, "Dynamic energy-efficient power allocation in multibeam satellite systems," *IEEE Wireless Commun. Lett.*, vol. 9, no. 2, pp. 228–231, Feb. 2020.

[11] A. I. Aravanis, B. Shankar M. R., P. Arapoglou, G. Danoy, P. G. Cottis, and B. Ottersten, "Power allocation in multibeam satellite systems: A two-stage multi-objective optimization," *IEEE Trans. Wireless Commun.*, vol. 14, no. 6, pp. 3171–3182, Jun. 2015.

[12] F. R. Durand and T. Abrão, "Power allocation in multibeam satellites based on particle swarm optimization," *AEU-Int. J. Electron. Commun.*, vol. 78, pp. 124–133, Aug. 2017. [Online]. Available: https://www.sciencedirect.com/science/article/pii/S1434841116303739

[13] S. Kisseleff, B. Shankar, D. Spano, and J.-D. Gayrard, "A new optimization tool for mega-constellation design and its application to trunking systems," in *Proc. 37th Int. Commun. Satellite Syst. Conf. Adv. Commun. Satellite Syst. (ICSSC)*, 2019, pp. 1–15.

[14] F. Li, K. Lam, X. Liu, J. Wang, K. Zhao, and L. Wang, "Joint pricing and power allocation for multibeam satellite systems with dynamic game model," *IEEE Trans. Veh. Technol.*, vol. 67, no. 3, pp. 2398–2408, Mar. 2018.

[15] J. J. G. Luis, M. Guerster, I. del Portillo, E. Crawley, and B. Cameron, "Deep reinforcement learning for continuous power allocation in flexible high throughput satellites," in *Proc. IEEE Cogn. Commun. Aerosp. Appl. Workshop (CCAAW)*, 2019, pp. 1–4.

[16] S. Liu, Y. Fan, Y. Hu, D. Wang, L. Liu, and L. Gao, "AG-DPA: Assignment game-based dynamic power allocation in multibeam satellite systems," *Int. J. Satellite Commun. Netw.*, vol. 38, no. 1, pp. 74–83, 2020. [Online]. Available: https://onlinelibrary.wiley.com/doi/abs/10.1002/sat.1310

[17] R. Chen, X. Hu, X. Li, and W. Wang, "Optimum power allocation based on traffic matching service for multi-beam satellite system," in *Proc. 5th Int. Conf. Comput. Commun. Syst. (ICCCS)*, 2020, pp. 655–659.

[18] P. Zhang, X. Wang, Z. Ma, S. Liu, and J. Song, "An Online power allocation algorithm based on deep reinforcement learning in multibeam satellite systems," *Int. J. Satellite Commun. Netw.*, vol. 38, no. 5, pp. 450–461, 2020. [Online]. Available: https://onlinelibrary.wiley.com/doi/abs/10.1002/sat.1352

[19] U. Park, H. W. Kim, D.-S. Oh, and B. J. Ku, "Flexible bandwidth allocation scheme based on traffic demands and channel conditions for multi-beam satellite systems," in *Proc. IEEE Veh. Technol. Conf.*, Sep. 2012, pp. 1–5.

[20] H. Wang, A. Liu, X. Pan, and L. Jia, "Optimal bandwidth allocation for multi-spot-beam satellite communication systems," in *Proc. Int. Conf. Mechatron. Sci. Elect. Eng. Comput. (MEC)*, 2013, pp. 2794–2798.

[21] X. Hu, S. Liu, R. Chen, W. Wang, and C. Wang, "A deep reinforcement learning-based framework for dynamic resource allocation in multibeam satellite systems," *IEEE Commun. Lett.*, vol. 22, no. 8, pp. 1612–1615, Aug. 2018.

[22] S. Liu, X. Hu, and W. Wang, "Deep reinforcement learning based dynamic channel allocation algorithm in multibeam satellite systems," *IEEE Access*, vol. 6, pp. 15733–15742, 2018.

[23] X. Hu *et al.*, "Multi-agent deep reinforcement learning-based flexible satellite payload for mobile terminals," *IEEE Trans. Veh. Technol.*, vol. 69, no. 9, pp. 9849–9865, Sep. 2020.

[24] X. Liao *et al.*, "Distributed intelligence: A verification for multi-agent DRL-based multibeam satellite resource allocation," *IEEE Commun. Lett.*, vol. 24, no. 12, pp. 2785–2789, Dec. 2020.

[25] J. Lei and M. A. Vázquez-Castro, "Joint power and carrier allocation for the multibeam satellite downlink with individual SINR constraints," in *Proc. IEEE Int. Conf. Commun.*, May 2010, pp. 1–5.

[26] G. Cocco, T. de Cola, M. Angelone, Z. Katona, and S. Erl, "Radio resource management optimization of flexible satellite payloads for DVB-S2 systems," *IEEE Trans. Broadcast.*, vol. 64, no. 2, pp. 266–280, Jun. 2018.

[27] A. Paris, I. Del Portillo, B. Cameron, and E. Crawley, "A genetic algorithm for joint power and bandwidth allocation in multibeam satellite systems," in *Proc. IEEE Aerosp. Conf.*, Mar. 2019, pp. 1–15.

[28] F. G. Ortiz-Gomez, D. Tarchi, R. Martínez, A. Vanelli-Coralli, M. A. Salas-Natera, and S. Landeros-Ayala, "Cooperative multi-agent deep reinforcement learning for resource management in full flexible VHTS systems," *IEEE Trans. Cogn. Commun. Netw.*, vol. 8, no. 1, pp. 335–349, Mar. 2022.

[29] F. G. Ortiz-Gomez, D. Tarchi, R. Martínez, A. Vanelli-Coralli, M. A. Salas-Natera, and S. Landeros-Ayala, "Convolutional neural networks for flexible payload management in VHTS systems," *IEEE Syst. J.*, vol. 15, no. 3, pp. 4675–4686, Sep. 2021.

[30] P. V. R. Ferreira *et al.*, "Multiobjective reinforcement learning for cognitive satellite communications using deep neural network ensembles," *IEEE J. Sel. Areas Commun.*, vol. 36, no. 5, pp. 1030–1041, May 2018.

[31] P. V. R. Ferreira *et al.*, "Reinforcement learning for satellite communications: From LEO to deep space operations," *IEEE Commun. Mag.*, vol. 57, no. 5, pp. 70–75, May 2019.

[32] T. S. Abdu, E. Lagunas, S. Kisseleff, and S. Chatzinotas, "Carrier and power assignment for flexible broadband GEO satellite communications system," in *Proc. IEEE 31st Annu. Int. Symp. Pers. Indoor Mobile Radio Commun.*, 2020, pp. 1–7.

[33] T. S. Abdu, S. Kisseleff, E. Lagunas, and S. Chatzinotas, "Limits of smart radio resource assignment in GEO satellite communications," in *Proc. IEEE Wireless Commun. Netw. Conf. (WCNC)*, 2021, pp. 1–7.

[34] T. S. Abdu, S. Kisseleff, E. Lagunas, and S. Chatzinotas, "Flexible resource optimization for GEO multibeam satellite communication system," *IEEE Trans. Wireless Commun.*, vol. 20, no. 12, pp. 7888–7902, Dec. 2021.

[35] "How Satellite Broadband Can Be a Game-Changer For Connected Planes: Report." [Online]. Available: https://news.itu.int/space-satellites-connected-planes/ (Accessed: Jul. 2021).

[36] L. Cottatellucci, M. Debbah, G. Gallinaro, R. Mueller, M. Neri, and R. Rinaldo, "Interference Mitigation Techniques for Broadband Satellite Systems." 2006. [Online]. Available: https://arc.aiaa.org/doi/abs/10.2514/6.2006–5348

[37] B. Devillers, A. Perez-Neira, and C. Mosquera, "Joint linear precoding and beamforming for the forward link of multi-beam broadband satellite systems," in *Proc. IEEE Global Telecommun. Conf. (GLOBECOM)*, 2011, pp. 1–6.

[38] G. Taricco, "Linear precoding methods for multi-beam broadband satellite systems," in *Proc. Eur. Wireless 20th Eur. Wireless Conf.*, 2014, pp. 1–6.

[39] "ESA LiveSatPreDem Project: Live Satellite Demonstration of Advanced Interference Management Techniques." [Online]. Available: https://artes.esa.int/projects/livesatpredem (Accessed: Jul. 2021.)

[40] E. Björnson, M. Bengtsson, and B. Ottersten, "Optimal multiuser transmit beamforming: A difficult problem with a simple solution structure [lecture notes]," *IEEE Signal Process. Mag.*, vol. 31, no. 4, pp. 142–148, Jul. 2014.

[41] G. Taricco and A. Ginesi, "Precoding for flexible high throughput satellites: Hot-spot scenario," *IEEE Trans. Broadcast.*, vol. 65, no. 1, pp. 65–72, Mar. 2019.

[42] D. Christopoulos, S. Chatzinotas, and B. Ottersten, "Weighted fair multicast multigroup beamforming under per-antenna power constraints," *IEEE Trans. Signal Process.*, vol. 62, no. 19, pp. 5132–5142, Oct. 2014.

[43] D. Christopoulos, S. Chatzinotas, and B. Ottersten, "Multicast multigroup precoding and user scheduling for frame-based satellite communications," *IEEE Trans. Wireless Commun.*, vol. 14, no. 9, pp. 4695–4707, Sep. 2015.

[44] J. Wang, L. Zhou, K. Yang, X. Wang, and Y. Liu, "Multicast precoding for multigateway multibeam satellite systems with feeder link interference," *IEEE Trans. Wireless Commun.*, vol. 18, no. 3, pp. 1637–1650, Mar. 2019.

[45] C. Qi and X. Wang, "Precoding design for energy efficiency of multibeam satellite communications," *IEEE Commun. Lett.*, vol. 22, no. 9, pp. 1826–1829, Sep. 2018.

[46] C. Qi, H. Chen, Y. Deng, and A. Nallanathan, "Energy efficient multicast precoding for multiuser multibeam satellite communications," *IEEE Wireless Commun. Lett.*, vol. 9, no. 4, pp. 567–570, Apr. 2020.

[47] P. J. Honnaiah, E. Lagunas, D. Spano, N. Maturo, and S. Chatzinotas, "Demand-based scheduling for precoded multibeam high-throughput satellite systems," in *Proc. IEEE Wireless Commun. Netw. Conf. (WCNC)*, 2021, pp. 1–6.

[48] L. Chen, E. Lagunas, S. Chatzinotas, and B. Ottersten, "Satellite broadband capacity-on-demand: Dynamic beam illumination with selective precoding," in *Proc. Eur. Signal Process. Conf. (EUSIPCO)*, 2021, pp. 900–904.

[49] A. Mengali, A. Ginesi, and S. D'Addio, "Computer-aided payload architecture optimization for HTS satellites," in *Proc. 10th Adv. Satellite Multimedia Syst. Conf. 16th Signal Process. Space Commun. Workshop (ASMS/SPSC)*, 2020, pp. 1–8.

[50] M. Á. Vázquez, X. Artiga, and A. I. Pérez-Neira, "Closed-form multicast precoding for satellite flexible payloads," in *Proc. 29th Eur. Signal Process. Conf. (EUSIPCO)*, 2021, pp. 910–914.

[51] S. Kisseleff *et al.*, "Centralized gateway concept for precoded multibeam GEO satellite networks," in *Proc. IEEE 94th Veh. Technol. Conf. (VTC2021-Fall)*, 2021, pp. 1–6.

[52] R. Marler and J. Arora, "Survey of multi-objective optimization methods for engineering," *Struct. Multidiscipl. Optim.*, vol. 26, no. 6, pp. 369–395, 2004.

[53] W. Dinkelbach, "On nonlinear fractional programming," *Manag. Sci.*, vol. 13, no. 7, pp. 492–498, 1967. [Online]. Available: http://www.jstor.org/stable/2627691

[54] S. Boyd and L. Vandenberghe, *Convex Optimization*. Cambridge, U.K.: Cambridge Univ. Press, 2004.

IEEE ComSoc

IEEE Open Journal of the
Communications Society

[55] K. Shen and W. Yu, "Fractional programming for communication systems–Part I: Power control and beamforming," *IEEE Trans. Signal Process.*, vol. 66, no. 10, pp. 2616–2630, May 2018.

[56] T. Wang and L. Vandendorpe, "Successive convex approximation based methods for dynamic spectrum management," in *Proc. IEEE Int. Conf. Commun. (ICC)*, 2012, pp. 4061–4065.

[57] M. Grant and S. Boyd, "CVX: MATLAB Software for Disciplined Convex Programming, Version 2.1," Mar. 2014. [Online]. Available: http://cvxr.com/cvx

[58] H. Al-Hraishawi, E. Lagunas, and S. Chatzinotas, "Traffic simulator for multibeam satellite communication systems," in *Proc. 10th Adv. Satellite Multimedia Syst. Conf. 16th Signal Process. Space Commun. Workshop (ASMS/SPSC)*, 2020, pp. 1–8.

[59] "Propagation data and prediction methods required for the design of earth-space telecommunication systems," Recommendation ITU-R, Geneva, Switzerland, ITU-R. 618-13 2017.

SYMEON CHATZINOTAS (Senior Member, IEEE) received the M.Eng. degree in telecommunications from the Aristotle University of Thessaloniki, Thessaloniki, Greece, in 2003, and the M.Sc. and Ph.D. degrees in electronic engineering from the University of Surrey, Surrey, U.K., in 2006 and 2009, respectively. He is currently a Full Professor/Chief Scientist I and the Head of the SIGCOM Research Group, SnT, University of Luxembourg. In the past, he was a Visiting Professor with the University of Parma, Italy, and he was involved in numerous research and development projects for the National Center for Scientific Research Demokritos, the Center for Research and Technology Hellas, and the Center of Communication Systems Research, University of Surrey. He has (co)authored more than 500 technical articles in refereed international journals, conferences, and scientific books. He was a co-recipient of the 2014 IEEE Distinguished Contributions to Satellite Communications Award, the CROWNCOM 2015, 2018 EURASIC JWCN and 2022 WCNC Paper Award. He is currently on the Editorial Board of the IEEE TRANSACTIONS ON COMMUNICATIONS, IEEE OPEN JOURNAL OF VEHICULAR TECHNOLOGY, and the *International Journal of Satellite Communications and Networking*.

TEDROS SALIH ABDU (Graduate Student Member, IEEE) received the joint M.Sc. degree in electrical engineering from Pan African University and Jomo Kenyatta University of Agriculture and Technology, Juja, in 2017. He is currently pursuing the Ph.D. degree with the Interdisciplinary Centre for Security, Reliability, and Trust, University of Luxembourg, where he is also a Doctoral Researcher. He has worked as a Lecturer with the Kombolcha Institute of Technology, Wollo University. His research interests include wireless communication technology, focusing on channel modeling, channel estimation, precoding, and resource optimization.

STEVEN KISSELEFF (Member, IEEE) received the M.Sc. degree in information technology from the Technical University of Kaiserslautern, Germany, in 2011, and the Ph.D. degree in electrical engineering from the Friedrich-Alexander University of Erlangen–Nürnberg (FAU), Germany, in 2017. He was a Research and Teaching Assistant with the Institute for Digital Communications, FAU from October 2011 to July 2018. In 2012 and 2013, he was a Visiting Researcher with the State University of New York at Buffalo, USA, and the Broadband Wireless Networking Lab, Georgia Institute of Technology, Atlanta, GA, USA. In 2018, he joined the Interdisciplinary Centre for Security, Reliability and Trust, University of Luxembourg, where he currently holds a research scientist position. His research activities are mainly focused on the satellite communications, wireless power transfer, symbol-level precoding, and reconfigurable intelligent surfaces.

BJÖRN OTTERSTEN (Fellow, IEEE) received the M.S. degree in electrical engineering and applied physics from Linköping University, Linköping, Sweden, in 1986, and the Ph.D. degree in electrical engineering from Stanford University, Stanford, CA, USA, in 1990. He has held research positions with the Department of Electrical Engineering, Linköping University, the Information Systems Laboratory, Stanford University, the Katholieke Universiteit Leuven, Leuven, Belgium, and the University of Luxembourg, Luxembourg. From 1996 to 1997, he was the Director of Research with ArrayComm, Inc., a start-up in San Jose, CA, USA, based on his patented technology. In 1991, he was appointed a Professor of Signal Processing with the Royal Institute of Technology (KTH), Stockholm, Sweden. He has been Head of the Department for Signals, Sensors, and Systems, KTH, and the Dean of the School of Electrical Engineering, KTH. He is currently the Director for the Interdisciplinary Centre for Security, Reliability and Trust, University of Luxembourg. He is a recipient of the IEEE Signal Processing Society Technical Achievement Award, the EURASIP Group Technical Achievement Award, and the European Research Council advanced research grant twice. He has co-authored journal papers that received the IEEE Signal Processing Society Best Paper Award in 1993, 2001, 2006, 2013, and 2019, and eight IEEE conference papers best paper awards. He has been a board member of IEEE Signal Processing Society, the Swedish Research Council and currently serves of the boards of EURASIP and the Swedish Foundation for Strategic Research. He has served as Editor-in-Chief for *EURASIP Signal Processing*, and acted on the editorial boards of IEEE TRANSACTIONS ON SIGNAL PROCESSING, *IEEE Signal Processing Magazine*, IEEE OPEN JOURNAL FOR SIGNAL PROCESSING, *EURASIP Journal on Advances in Signal Processing*, and *Foundations and Trends in Signal Processing*. He is a Fellow of EURASIP.

EVA LAGUNAS (Senior Member, IEEE) received the M.Sc. and Ph.D. degrees in telecommunications engineering from the Polytechnic University of Catalonia, Barcelona, Spain, in 2010 and 2014, respectively, where she was a Research Assistant with the Department of Signal Theory and Communications from 2009 to 2013. In Summer 2009, she was a Guest Research Assistant with the Department of Information Engineering, Pisa, Italy. From November 2011 to May 2012, she held a visiting research appointment with the Center for Advanced Communications, Villanova University, Villanova, PA, USA. In 2014, she joined the Interdisciplinary Centre for Security, Reliability and Trust, University of Luxembourg, where she currently holds a research scientist position. Her research interests include radio resource management and general wireless networks optimization.